TABLE IV—*continued*

Gene name	C/P	*p* Value	Cm/C	*p* Value	Cm/P	*p* Value
COL3A1	1.24	0.642	1.34	0.517	1.67	0.212
POSTN	0.90	0.687	1.94	0.018	1.75	0.033
NT5E	1.05	0.802	1.21	0.473	1.27	0.329
PEX13	1.73	<0.01	0.81	0.224	1.40	0.025
UBAC2	1.87	<0.01	0.95	0.834	1.78	0.044
TLCD1	2.13	<0.01	0.76	0.335	1.63	0.113
SERPIND1	1.57	0.018	1.21	0.371	1.90	<0.01
SLC2A1	2.57	0.175	1.18	0.758	3.03	0.051
FAM173A	1.18	0.433	0.81	0.259	0.96	0.860
TMEM45B	1.35	0.255	0.97	0.918	1.30	0.400

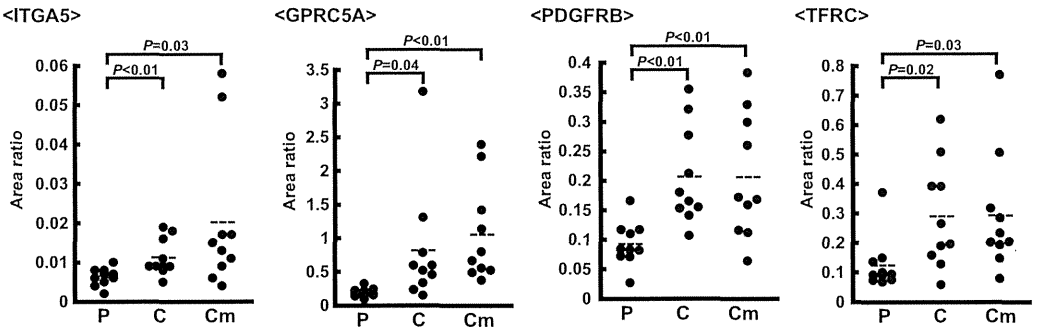

FIG. 3. **Representative results of SRM/MRM in the verification step.** The SRM/MRM data of ITGA5, GPRC5A, PDGFRB, and TFRC are shown. P, polyp. C, cancer without metastasis. Cm, cancer with metastasis. Area ratio, the ratio of the peak area of the endogenous peptide to that of the SI peptide.

proteins identified because of the absence of an appropriate validation method. SRM/MRM was recently shown to be an efficient validation method (3–5) and several studies, including our own, reported the identification of biomarker candidates by quantitative shotgun proteomics using the iTRAQ labeling method and verification by SRM/MRM (19, 21, 33). In the present study, we performed a proteomic analysis of membrane fractions prepared from colorectal cancer tissue to identify novel biomarker candidates for diagnosis and/or therapeutic targets. We identified membrane proteins, the expression levels of which were altered with the development and progression of colorectal cancer, using comprehensive quantitative analysis with iTRAQ. The most significant achievement of this study was the SRM/MRM-based confirmation and simultaneous large-scale verification using an independent set of tissue samples. Of the 105 biomarker candidate proteins identified by iTRAQ, changes in the expression of 69 proteins were confirmed by SRM/MRM, with significant differences being verified in 44 proteins between groups. This discovery-confirmation-verification workflow should be able to identify more reliable biomarkers for the clinical diagnosis of colon cancer. To the best of our knowledge, we have performed the largest verification of biomarker candidate membrane proteins to date. This verification process using SRM/MRM enabled us to select more potential candidates and prioritize the subsequent validation, and may represent a rapid and effective method to identify novel biomarkers.

We were able to identify 5566 proteins in the membrane fraction in the present study, 3087 (58.4%) of which were predicted to be membrane proteins. This number was markedly higher than that previously reported (34–38); however, non-membrane proteins were also identified in addition to membrane proteins, and this was attributed to the preparation of crude membrane fractions using a simple method. One of the reasons for the increased rate of membrane protein identification was the PTS method-based isolation of membrane proteins (12, 13). The PTS method enables the efficient isolation of membrane proteins and allows the use of a high detergent concentration to achieve the efficient solubilization of very hydrophobic membrane proteins in the cleavage procedure of membrane proteins. Thus, this method may provide deeper proteome coverage for the identification of tissue membrane proteins.

We focused on membrane proteins in this study because membrane proteins are not only involved in the regulation of cell signaling and cell-cell interactions, but are also suitable therapeutic targets for cancers (39). One of the greatest advances in the treatment of cancer in recent years has been the discovery of molecular-targeted drugs, which has resulted in the development of many antibody drugs. Membrane proteins are clearly the best targets for antibody drugs. In this study, we identified a number of previously unreported membrane proteins, the expression of which changed with the development and progression of colorectal cancer. These membrane

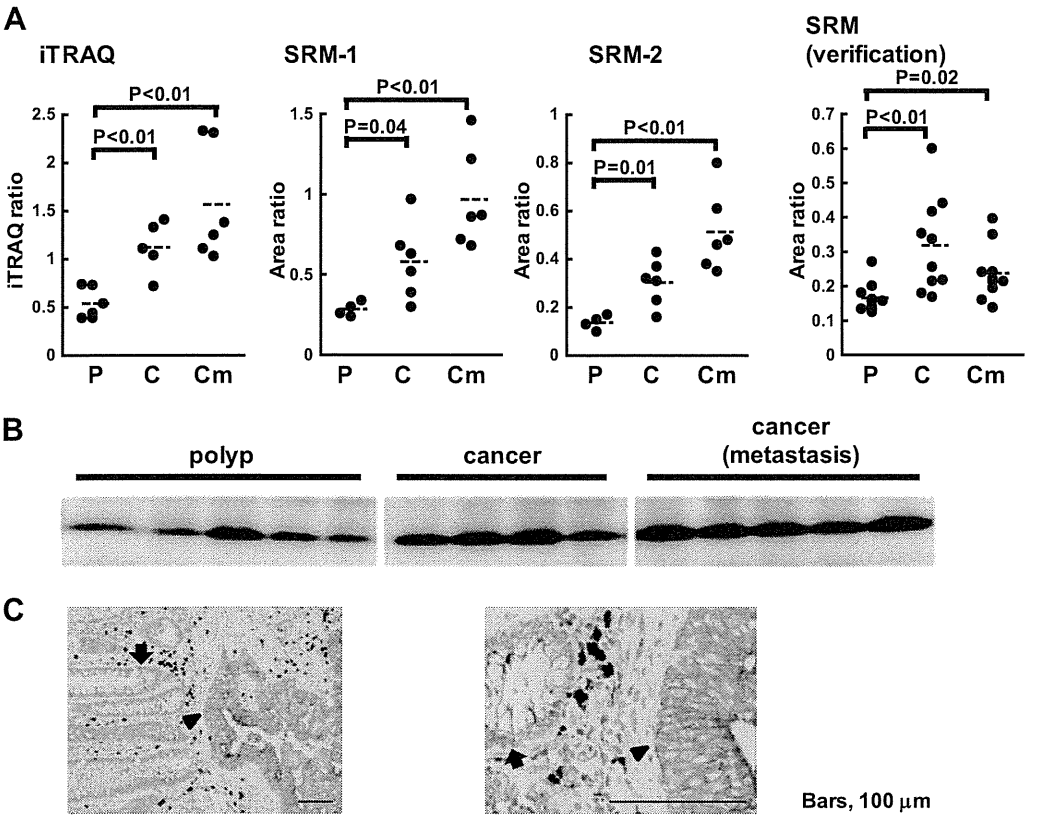

FIG. 4. **Validation of the biomarker candidate C8orf55**. *A*, The iTRAQ and SRM/MRM data of C8orf55. P, polyp. C, cancer without metastasis. Cm, cancer with metastasis. Area ratio, the ratio of the peak area of the endogenous peptide to that of the SI peptide. Assays were constructed to measure two distinct peptides per-protein listed in supplemental Table S5 and that the individual assays for each of the two peptides are labeled SRM-1 and SRM-2. *B*, Western blotting analysis of polyps and cancer with and without metastasis using an anti-C8orf55 antibody. *C*, Immunohistochemical staining of colorectal cancer tissue using an anti-C8orf55 antibody. *Left* panel: lower magnification. *Right* panel: higher magnification. The arrowhead shows areas of stained tumor cells and the arrow shows normal colon epithelial glands. Bar, 100 μm.

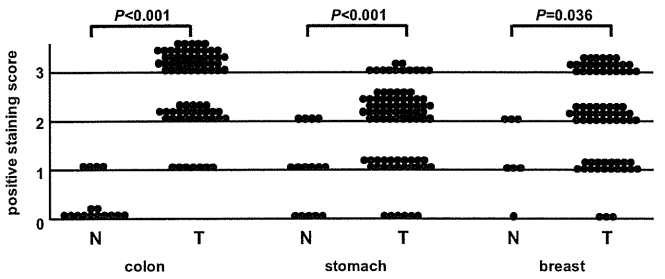

FIG. 5. **Tissue microarray of C8orf55**. C8orf55 immunohistochemistry score (staining intensity) between normal and cancer tissues. Statistical analyses were performed using the Wilcoxon test.

proteins may be novel therapeutic targets for antibody drug discovery.

Membrane proteins are also suitable biomarkers for the screening and diagnosis of various cancers. Diagnostic biomarkers are ideally detected and quantified in biological fluids such as the plasma and/or urine; however, soluble proteins derived from tissue leakage are often very difficult to detect because there are very few and they are unstable. In contrast, membrane proteins and extracellular proteins are potentially shed and secreted from cells into the circulation; some are actively secreted as microvesicles, such as exosomes, which are very stable and may be potential biomarkers. Several previous studies reported the potential for diagnosing malignant tumors, such as colorectal cancer, melanoma, and glioblastoma, by analyzing exosomal proteins (40–42). Thus, the membrane proteins identified in this study may be promising biomarker candidates for the diagnosis of colorectal cancer.

We observed variations in the quantitative results obtained from iTRAQ and SRM. The samples used for iTRAQ were fractionated with a SCX column, while those for SRM were not. Therefore, variations may have occurred in the quantitative results obtained from iTRAQ and SRM because of differences in the complexities of the samples analyzed. Splicing isoforms or post-translational modifications may also have been involved in these variations because iTRAQ ratios were calculated as the average of all contributing peptide iTRAQ measurements and SRM ratios were obtained by measuring a target peptide.

We investigated differences in the expression levels of proteins between polyps and cancer tissues without metastasis in the present study using proteomic analysis to identify characteristic expression profiles in cancer. Although a number of

previous biomarker studies identified hundreds of candidate proteins by comparing cancer tissues with matched normal tissues, many proteins unrelated to malignant properties may also have been included because cancer is generally not directly derived from normal tissues. Thus, the best negative control would be benign tumors, ideally premalignant lesions. In this regard, colorectal polyps are considered to be the best control for colorectal cancer. Moreover, a comparison between different stages of cancer tissues, including benign tumors, is the optimal procedure to identify more useful biomarker candidates.

In our study, C8orf55 was confirmed by SRM/MRM and Western blotting, the findings of which were further verified by multiple cancer tissue microarrays (TMA1150). TMA1150 had 1150 cores from 50 or 100 cases of 14 cancer types and was previously shown to be useful for evaluating changes in protein expression in multiple cancers (25). TMA1150 can also be used to examine the expression of target proteins in various cancer tissues as well as in dozens of cases of colorectal cancer. The extensive validation of the expression of identified candidates in various types of cancer tissues is important in order to determine their usefulness as biomarkers for diverse cancers. In this regard, multi-cancer TMA is a very effective method that can be used to rapidly and simply evaluate the expression patterns of various cancers. TMA1150 revealed that the expression of C8orf55 was higher not only in colon cancer tissue, but also in other cancer tissues, which suggested that these proteins have the potential to be biomarkers for stomach and breast cancer as well as colon cancer.

In conclusion, we successfully performed a SRM/MRM-based large-scale verification of biomarker candidate membrane proteins for colorectal cancer tissues. The methods described here can be readily applied to any type of cancer tissue and can contribute to the identification of novel biomarkers for the diagnosis and therapeutic targets of diseases.

Acknowledgments—The mass spectrometry proteomics data have been deposited to the ProteomeXchange Consortium (http://proteomecentral.proteomexchange.org) via the PRIDE partner repository (43) with the dataset identifier PXD000851.

* This work was supported by a Grant-in-Aid, Research on Biological Markers for New Drug Development H20–0005, to T.T. from the Ministry of Health, Labor and Welfare of Japan. It was also supported by Grants-in-Aid 21390354 to T.T and 22590545 to H.K. from the Ministry of Education, Science, Sports and Culture of Japan.

[S] This article contains supplemental Figs. S1 to S6 and Tables S1 to S9.

|||| To whom correspondence should be addressed: Laboratory of Proteome Research, National Institute of Biomedical Innovation, 7-6-8 Saito-Asagi, Ibaraki-shi, Osaka 567–0085, Japan. Tel.: +81-72-641-9862; Fax: +81-72-641-9861; E-mail: tomonaga@nibio.go.jp.

REFERENCES

1. Ross, P. L., Huang, Y. N., Marchese, J. N., Williamson, B., Parker, K., Hattan, S., Khainovski, N., Pillai, S., Dey, S., Daniels, S., Purkayastha, S., Juhasz, P., Martin, S., Bartlet-Jones, M., He, F., Jacobson, A., and Pappin, D. J. (2004) Multiplexed protein quantitation in *Saccharomyces cerevisiae* using amine-reactive isobaric tagging reagents, *Mol. Cell. Proteomics* **3,** 1154–1169
2. Ong, S. E., Blagoev, B., Kratchmarova, I., Kristensen, D. B., Steen, H., Pandey, A., and Mann, M. (2002) Stable isotope labeling by amino acids in cell culture, SILAC, as a simple and accurate approach to expression proteomics. *Mol. Cell. Proteomics* **1,** 376–386
3. Whiteaker, J. R., Zhang, H., Zhao, L., Wang, P., Kelly-Spratt, K. S., Ivey, R. G., Piening, B. D., Feng, L. C., Kasarda, E., Gurley, K. E., Eng, J. K., Chodosh, L. A., Kemp, C. J., McIntosh, M. W., and Paulovich, A. G. (2007) Integrated pipeline for mass spectrometry-based discovery and confirmation of biomarkers demonstrated in a mouse model of breast cancer. *J. Proteome Res.* **6,** 3962–3975
4. Keshishian, H., Addona, T., Burgess, M., Mani, D. R., Shi, X., Kuhn, E., Sabatine, M. S., Gerszten, R. E., and Carr, S. A. (2009) Quantification of cardiovascular biomarkers in patient plasma by targeted mass spectrometry and stable isotope dilution. *Mol. Cell. Proteomics* **8,** 2339–2349
5. Whiteaker, J. R., Lin, C., Kennedy, J., Hou, L., Trute, M., Sokal, I., Yan, P., Schoenherr, R. M., Zhao, L., Voytovich, U. J., Kelly-Spratt, K. S., Krasnoselsky, A., Gafken, P. R., Hogan, J. M., Jones, L. A., Wang, P., Amon, L., Chodosh, L. A., Nelson, P. S., McIntosh, M. W., Kemp, C. J., and Paulovich, A. G. (2011) A targeted proteomics-based pipeline for verification of biomarkers in plasma. *Nat. Biotechnol.* **29,** 625–634
6. Ahram, M., Litou, Z. I., Fang, R., and Al-Tawallbeh, G. (2006) Estimation of membrane proteins in the human proteome. *In Silico Biol.* **6,** 379–386
7. Hopkins, A. L., and Groom, C. R. (2002) The druggable genome. *Nat. Rev. Drug Discovery* **1,** 727–730
8. Chen, E. I., Cociorva, D., Norris, J. L., and Yates, J. R., 3rd. (2007) Optimization of mass spectrometry-compatible surfactants for shotgun proteomics. *J. Proteome Res.* **6,** 2529–2538
9. Mitra, S. K., Gantt, J. A., Ruby, J. F., Clouse, S. D., and Goshe, M. B. (2007) Membrane proteomic analysis of *Arabidopsis thaliana* using alternative solubilization techniques. *J. Proteome Res.* **6,** 1933–1950
10. Zhang, N., Chen, R., Young, N., Wishart, D., Winter, P., Weiner, J. H., and Li, L. (2007) Comparison of SDS- and methanol-assisted protein solubilization and digestion methods for *Escherichia coli* membrane proteome analysis by 2-D LC-MS/MS. *Proteomics* **7,** 484–493
11. Zhou, J., Zhou, T., Cao, R., Liu, Z., Shen, J., Chen, P., Wang, X., and Liang, S. (2006) Evaluation of the application of sodium deoxycholate to proteomic analysis of rat hippocampal plasma membrane. *J. Proteome Res.* **5,** 2547–2553
12. Masuda, T., Tomita, M., and Ishihama, Y. (2008) Phase transfer surfactant-aided trypsin digestion for membrane proteome analysis. *J. Proteome Res.* **7,** 731–740
13. Masuda, T., Saito, N., Tomita, M., and Ishihama, Y. (2009) Unbiased quantitation of *Escherichia coli* membrane proteome using phase transfer surfactants. *Mol. Cell. Proteomics* **8,** 2770–2777
14. Tomonaga, T., Matsushita, K., Yamaguchi, S., Oh-Ishi, M., Kodera, Y., Maeda, T., Shimada, H., Ochiai, T., and Nomura, F. (2004) Identification of altered protein expression and post-translational modifications in primary colorectal cancer by using agarose two-dimensional gel electrophoresis. *Clin. Cancer Res.* **10,** 2007–2014
15. Nishimori, T., Tomonaga, T., Matsushita, K., Oh-Ishi, M., Kodera, Y., Maeda, T., Nomura, F., Matsubara, H., Shimada, H., and Ochiai, T. (2006) Proteomic analysis of primary esophageal squamous cell carcinoma reveals downregulation of a cell adhesion protein, periplakin. *Proteomics* **6,** 1011–1018
16. Seimiya, M., Tomonaga, T., Matsushita, K., Sunaga, M., Oh-Ishi, M., Kodera, Y., Maeda, T., Takano, S., Togawa, A., Yoshitomi, H., Otsuka, M., Yamamoto, M., Nakano, M., Miyazaki, M., and Nomura, F. (2008) Identification of novel immunohistochemical tumor markers for primary hepatocellular carcinoma; clathrin heavy chain and formiminotransferase cyclodeaminase. *Hepatology* **48,** 519–530
17. Katada, K., Tomonaga, T., Satoh, M., Matsushita, K., Tonoike, Y., Kodera, Y., Hanazawa, T., Nomura, F., and Okamoto, Y. (2012) Plectin promotes migration and invasion of cancer cells and is a novel prognostic marker for head and neck squamous cell carcinoma. *J. Proteomics* **75,** 1803–1815
18. Lazebnik, Y. (2010) What are the hallmarks of cancer? *Nat. Rev. Cancer* **10,** 232–233
19. Muraoka, S., Kume, H., Watanabe, S., Adachi, J., Kuwano, M., Sato, M.,

Kawasaki, N., Kodera, Y., Ishitobi, M., Inaji, H., Miyamoto, Y., Kato, K., and Tomonaga, T. (2012) Strategy for SRM-based verification of biomarker candidates discovered by iTRAQ method in limited breast cancer tissue samples. *J. Proteome Res.* **11,** 4201–4210

20. Muraoka, S., Kume, H., Adachi, J., Shiromizu, T., Watanabe, S., Masuda, T., Ishihama, Y., and Tomonaga, T. (2013) In-depth membrane proteomic study of breast cancer tissues for the generation of a chromosome-based protein list. *J. Proteome Res.* **12,** 208–213
21. Narumi, R., Murakami, T., Kuga, T., Adachi, J., Shiromizu, T., Muraoka, S., Kume, H., Kodera, Y., Matsumoto, M., Nakayama, K., Miyamoto, Y., Ishitobi, M., Inaji, H., Kato, K., and Tomonaga, T. (2012) A strategy for large-scale phosphoproteomics and SRM-based validation of human breast cancer tissue samples. *J. Proteome Res.* **11,** 5311–5322
22. Shiromizu, T., Adachi, J., Watanabe, S., Murakami, T., Kuga, T., Muraoka, S., and Tomonaga, T. (2013) Identification of missing proteins in the nextprot database and unregistered phosphopeptides in the phosphositeplus database as part of the chromosome-centric human proteome project. *J. Proteome Res.* DOI 10.1021/pr300825v
23. Rappsilber, J., Ishihama, Y., and Mann, M. (2003) Stop and go extraction tips for matrix-assisted laser desorption/ionization, nanoelectrospray, and LC/MS sample pretreatment in proteomics. *Anal. Chem.* **75,** 663–670
24. Selevsek, N., Matondo, M., Sanchez Carbayo, M., Aebersold, R., and Domon, B. Systematic quantification of peptides/proteins in urine using selected reaction monitoring. *Proteomics* **11,** 1135–1147
25. Kitano, H., Kageyama, S., Hewitt, S. M., Hayashi, R., Doki, Y., Ozaki, Y., Fujino, S., Takikita, M., Kubo, H., and Fukuoka, J. (2010) Podoplanin expression in cancerous stroma induces lymphangiogenesis and predicts lymphatic spread and patient survival. *Arch. Pathol. Lab Med.* **134,** 1520–1527
26. Yang, B., Gao, J., Rao, Z., and Shen, Q. (2013) Clinicopathological and Prognostic Significance of alpha5beta1-integrin and MMP-14 Expressions in Colorectal Cancer. *Neoplasma* DOI 10.4149/neo_2013_034
27. Zougman, A., Hutchins, G. G., Cairns, D. A., Verghese, E., Perry, S. L., Jayne, D. G., Selby, P. J., and Banks, R. E. (2013) Retinoic acid-induced protein 3: identification and characterisation of a novel prognostic colon cancer biomarker. *Eur. J. Cancer* **49,** 531–539
28. Sillars-Hardebol, A. H., Carvalho, B., de Wit, M., Postma, C., Delis-van Diemen, P. M., Mongera, S., Ylstra, B., van de Wiel, M. A., Meijer, G. A., and Fijneman, R. J. (2010) Identification of key genes for carcinogenic pathways associated with colorectal adenoma-to-carcinoma progression. *Tumour Biol.* **31,** 89–96
29. Prutki, M., Poljak-Blazi, M., Jakopovic, M., Tomas, D., Stipancic, I., and Zarkovic, N. (2006) Altered iron metabolism, transferrin receptor 1 and ferritin in patients with colon cancer. *Cancer Lett.* **238,** 188–196
30. Luo, Y., Wang, L., and Wang, J. (2013) Developing proteomics-based biomarkers for colorectal neoplasms for clinical practice: Opportunities and challenges. *Proteomics Clin. Appl.* **7,** 30–41
31. Lehtio, J., and De Petris, L. (2010) Lung cancer proteomics, clinical and technological considerations. *J. Proteomics* **73,** 1851–1863
32. Kalinina, J., Peng, J., Ritchie, J. C., and Van Meir, E. G. (2011) Proteomics of gliomas: initial biomarker discovery and evolution of technology *Neuro Oncol.* **13,** 926–942
33. Thingholm, T. E., Bak, S., Beck-Nielsen, H., Jensen, O. N., and Gaster, M. (2011) Characterization of human myotubes from type 2 diabetic and nondiabetic subjects using complementary quantitative mass spectrometric methods. *Mol. Cell. Proteomics* **10,** DOI 10.1074/mcp.M110.006650
34. Josic, D., and Clifton, J. G. (2007) Mammalian plasma membrane proteomics. *Proteomics* **7,** 3010–3029
35. Chen, J. S., Chen, K. T., Fan, C. W., Han, C. L., Chen, Y. J., Yu, J. S., Chang, Y. S., Chien, C. W., Wu, C. P., Hung, R. P., and Chan, E. C. (2010) Comparison of membrane fraction proteomic profiles of normal and cancerous human colorectal tissues with gel-assisted digestion and iTRAQ labeling mass spectrometry. *FEBS J.* **277,** 3028–3038
36. Han, C. L., Chen, J. S., Chan, E. C., Wu, C. P., Yu, K. H., Chen, K. T., Tsou, C. C., Tsai, C. F., Chien, C. W., Kuo, Y. B., Lin, P. Y., Yu, J. S., Hsueh, C., Chen, M. C., Chan, C. C., Chang, Y. S., and Chen, Y. J. (2011) An informatics-assisted label-free approach for personalized tissue membrane proteomics: case study on colorectal cancer. *Mol. Cell. Proteomics* 10, DOI 10.1074/mcp.M110.003087
37. Besson, D., Pavageau, A. H., Valo, I., Bourreau, A., Belanger, A., Eymerit-Morin, C., Mouliere, A., Chassevent, A., Boisdron-Celle, M., Morel, A., Solassol, J., Campone, M., Gamelin, E., Barre, B., Coqueret, O., and Guette, C. (2011) A quantitative proteomic approach of the different stages of colorectal cancer establishes OLFM4 as a new nonmetastatic tumor marker. *Mol. Cell. Proteomics* **10,** DOI 10.1074/mcp.M111.009712
38. Polisetty, R. V., Gautam, P., Sharma, R., Harsha, H. C., Nair, S. C., Gupta, M. K., Uppin, M. S., Challa, S., Puligopu, A. K., Ankathi, P., Purohit, A. K., Chandak, G. R., Pandey, A., and Sirdeshmukh, R. (2012) LC-MS/MS analysis of differentially expressed glioblastoma membrane proteome reveals altered calcium signaling and other protein groups of regulatory functions. *Mol. Cell. Proteomics* **11,** DOI 10.1074/mcp.M111.013565
39. Rucevic, M., Hixson, D., and Josic, D. (2011) Mammalian plasma membrane proteins as potential biomarkers and drug targets. *Electrophoresis* **32,** 1549–1564
40. Choi, D. S., Park, J. O., Jang, S. C., Yoon, Y. J., Jung, J. W., Choi, D. Y., Kim, J. W., Kang, J. S., Park, J., Hwang, D., Lee, K. H., Park, S. H., Kim, Y. K., Desiderio, D. M., Kim, K. P., and Gho, Y. S. (2011) Proteomic analysis of microvesicles derived from human colorectal cancer ascites. *Proteomics* **11,** 2745–2751
41. Peinado, H., Aleckovic, M., Lavotshkin, S., Matei, I., Costa-Silva, B., Moreno-Bueno, G., Hergueta-Redondo, M., Williams, C., Garcia-Santos, G., Ghajar, C., Nitadori-Hoshino, A., Hoffman, C., Badal, K., Garcia, B. A., Callahan, M. K., Yuan, J., Martins, V. R., Skog, J., Kaplan, R. N., Brady, M. S., Wolchok, J. D., Chapman, P. B., Kang, Y., Bromberg, J., and Lyden, D. (2012) Melanoma exosomes educate bone marrow progenitor cells toward a pro-metastatic phenotype through MET. *Nat. Med.* **18,** 883–891
42. Shao, H., Chung, J., Balaj, L., Charest, A., Bigner, D. D., Carter, B. S., Hochberg, F. H., Breakefield, X. O., Weissleder, R., and Lee, H. (2012) Protein typing of circulating microvesicles allows real-time monitoring of glioblastoma therapy. *Nat. Med.* **18,** 1835–1840
43. Vizcaino, J. A., Cote, R. G., Csordas, A., Dianes, J. A., Fabregat, A., Foster, J. M., Griss, J., Alpi, E., Birim, M., Contell, J., O'Kelly, G., Schoenegger, A., Ovelleiro, D., Perez-Riverol, Y., Reisinger, F., Rios, D., Wang, R., and Hermjakob, H. (2013) The PRoteomics IDEntifications (PRIDE) database and associated tools: status in 2013. *Nucleic Acids Res.* **41,** D1063–1069

Journal of proteome research

Article

pubs.acs.org/jpr

Absolute Quantitation of Low Abundance Plasma APL1β peptides at Sub-fmol/mL Level by SRM/MRM without Immunoaffinity Enrichment

Shozo Sano,[†] Shinji Tagami,[‡] Yuuki Hashimoto,[†] Kumiko Yoshizawa-Kumagaye,[§] Masahiko Tsunemi,[§] Masayasu Okochi,[‡] and Takeshi Tomonaga*,[†]

[†]Laboratory of Proteome Research, National Institute of Biomedical Innovation, Osaka 567-0085, Japan

[‡]Psychiatry, Department of Integrated Medicine, Division of Internal Medicine, Osaka University Graduate School of Medicine, Osaka 565-0871, Japan

[§]Peptide Institute, Inc., Osaka 562-8686, Japan

S *Supporting Information*

ABSTRACT: Selected/multiple reaction monitoring (SRM/MRM) has been widely used for the quantification of specific proteins/peptides, although it is still challenging to quantitate low abundant proteins/peptides in complex samples such as plasma/serum. To overcome this problem, enrichment of target proteins/peptides is needed, such as immunoprecipitation; however, this is labor-intense and generation of antibodies is highly expensive. In this study, we attempted to quantify plasma low abundant APLP1-derived Aβ-like peptides (APL1β), a surrogate marker for Alzheimer's disease, by SRM/MRM using stable isotope-labeled reference peptides without immunoaffinity enrichment. A combination of Cibacron Blue dye mediated albumin removal and acetonitrile extraction followed by C_{18}-strong cation exchange multi-StageTip purification was used to deplete plasma proteins and unnecessary peptides. Optimal and validated precursor ions to fragment ion transitions of APL1β were developed on a triple quadruple mass spectrometer, and the nanoliquid chromatography gradient for peptide separation was optimized to minimize the biological interference of plasma. Using the stable isotope-labeled (SI) peptide as an internal control, absolute concentrations of plasma APL1β peptide could be quantified as several hundred amol/mL. To our knowledge, this is the lowest detection level of endogenous plasma peptide quantified by SRM/MRM.

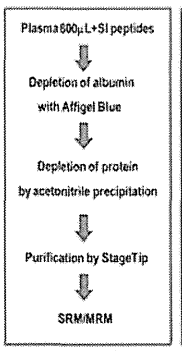

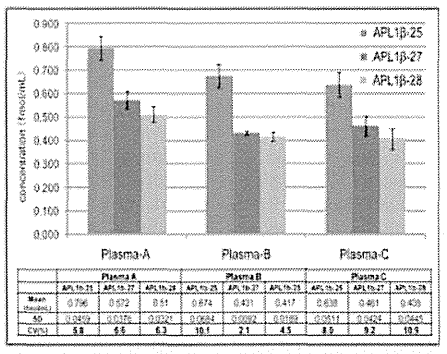

KEYWORDS: *SRM/MRM, low abundant plasma peptide, peptide enrichment, Alzheimer's disease*

INTRODUCTION

Recent advances in proteomic technology have made it possible to quantitate biomarker candidate proteins/peptides using selected/multiple reaction monitoring (SRM/MRM), a very sensitive mass spectrometric technique for the detection and quantification of targeted proteins and peptides.[1] Suitable sets of precursor and fragment ion masses for a given peptide, called SRM/MRM transitions, constitute definitive mass spectrometry assays that identify peptides and the corresponding proteins. More recently, SRM/MRM using stable isotope peptides has been adapted to measure the concentrations of candidate protein/peptide biomarkers in cell lysates as well as human plasma and serum.[2−5]

Although SRM/MRM is a very sensitive mass spectrometric technique, human plasma and serum are the most challenging biospecimens for the detection and quantitation of protein/peptide biomarkers due to highly abundant proteins such as albumin and immunoglobulin that impede the detection of low abundant proteins/peptides. A common approach to deplete plasma/serum abundant proteins is the use of immunodepletion, which specifically removes high abundance proteins such as albumin, transferrin, and immunoglobulins. Although previous reports efficiently removed high abundance plasma proteins using IgY14 or SuperMix,[6,7] other highly abundant proteins still existed in the flow-through fraction. Therefore, an additional enrichment step must be added to quantify candidate biomarkers present at lower concentrations in plasma/serum. Targeted enrichment has been performed with or without antibodies to improve the sensitivity of quantitation. Recently, a combination of the immunoaffinity approach with SRM/MRM using stable isotope peptides, such as SISCAPA-SRM, immuno-SRM, and mass spectrometric immunoassay (MSIA), significantly improved the quantification of low abundant protein

Received: October 8, 2013
Published: December 19, 2013

biomarkers present in plasma.[8−13] Using the MSIA method, the lowest detection level (LOQ) of plasma proteins is 16−31 pg/mL.[13] However, antibodies of proteins/peptides of interest are not always commercially available and there is no guarantee of being able to obtain suitable antibodies for immunoprecipitation if they are developed in-house. Therefore, antibody-free enrichment of target proteins has recently been applied for the quantitation of low abundant plasma proteins and demonstrated accurate and reproducible quantification of proteins at concentrations in the 50−100 pg/mL range.[14]

A key feature of the pathology of Alzheimer's disease (AD) is the accumulation of amyloid-β peptides (Aβ) in senile plaques and Aβ42 is its major constituent.[15,16] Thus, the level of Aβ42, especially relative to total Aβ in the brain, is a potential biomarker of AD. However, since Aβ42 is cleared more rapidly from the soluble pool in the brain by an enhanced rate of deposition/aggregation,[17−19] it is hardly detected in body fluid such as CSF and plasma, and surrogate markers for estimating Aβ42 generation in the brain have not yet been identified. We have previously identified novel APLP1-derived Aβ-like (APL1β) peptides, APL1β 25, 27, 28, that consist of 25−28 amino acids, in human CSF[20,21] and demonstrated that the CSF APL1β28 level is a potential surrogate marker for brain Aβ42 production. Moreover, the relative APL1β28 level as compared with total APL1β peptides is higher in CSF from sporadic AD patients than from non-AD controls, which is a potential biomarker for AD. However, examination of CSF is highly invasive for medical screening and a less aggressive procedure such as a blood test is needed.

Various methods have been used to analyze low molecular weight peptides in plasma/serum, including ultrafiltration, organic precipitation, and solid-phase extraction cartridges.[22−25] However, the most suitable method for analysis depends on the peptides to be analyzed. Several endogenous peptides in plasma or serum, such as human parathyroid hormone, insulin, and gastric inhibitory polypeptides, have been recently quantified by SRM/MRM, and the LOQ of the peptides was 1−18 fmol/mL.[26−28] In this study, we combined Cibacron Blue F3GA dye mediated albumin removal (Affi-Gel Blue; Bio-Rad, Hercules, CA) and acetonitrile (ACN) extraction to deplete plasma/serum proteins for SRM/MRM analysis of APL1β peptides. We also used C18-SCX multi-StageTips for removing unnecessary peptides.[29] Using 800 μL of plasma, endogenous APL1β peptides were able to be detected and quantified by SRM/MRM without immunoaffinity enrichment of the peptides. Strikingly, the absolute concentration of APL1β peptides was identified as several hundred amol/mL, which is the lowest detection level of endogenous plasma peptides to our knowledge.

MATERIALS AND METHODS

Synthetic Peptides

APL1β25, 27, 28 synthetic peptides were described previously.[21] Stable isotope-labeled peptides (SI peptides) for APL1β25, 27, 28 with a ^{15}N- and ^{13}C-labeled leucine[3] were synthesized at the Peptide Institute, Inc. (Osaka, Japan) using the t-butyloxycarbonyl (Boc) strategy and purified by reversed-phase (RP) HPLC. The labeled starting material, Boc-Leu(U−$^{13}C_6$, ^{15}N) (isotopic purity: 98%), was purchased from Cambridge Isotope Laboratories (Andover, MA). The chemical purity of these peptides was more than 98% determined by RP-HPLC and/or by capillary zone electrophoresis. The exact quantities of the synthetic peptides were determined by amino acid analysis of their acid hydrolysates in order to apply them to absolute quantitation of APL1β peptides in human plasma.

Collection of Human Plasma

Blood samples were collected from healthy volunteers at Osaka University Hospital. All the experiments using plasma were approved by the ethics committee of Osaka University Hospital (Nos. 07139 and 07212). Blood samples were centrifuged for 10 min at 3000*g*, and aliquots of the plasma supernatants were frozen immediately at −80 °C. The plasma samples were frozen and thawed once or twice before measurement.

Pretreatment of Plasma, Albumin Depletion, and ACN Precipitation

Human plasma samples were pretreated using Affi-Gel Blue and Mini Bio-Spin Chromatography Columns (Bio-Rad, Hercules, CA) according to the manufacturer's instructions. Briefly, 800 μL of plasma was diluted with an equal volume of 25 mM K_2HPO_4 and 0.1% *n*-octyl-β-glucoside (pH 7.0), and the SI peptide mixture was added to the pretreated samples at 5 fmol/mL. The sample was loaded onto a 1 mL Affi-Gel Blue column and vigorously mixed for 10 min at room temperature. The column was centrifuged for 1 min at 10 000*g*, and the eluate was applied to a new Affi-Gel Blue column, vigorously mixed for 10 min at room temperature, and centrifuged, and then the eluate was collected.

ACN was added to the eluate at several concentrations, as indicated in the text and in Figure 2, and centrifuged for 10 min at 20 000*g*. The supernatant was dried with a SpeedVac and resuspended with 100 μL of 40% ACN and 0.1% trifluoroacetic acid (TFA) and incubated for 3 or 5 min at room temperature. The sample was diluted with an equal volume of distilled water and centrifuged for 10 min at 20 000*g*. A volume of 5 μL of TFA was added to the supernatant and subjected to the following procedures.

StageTip Purification of Pretreated Plasma

To make the C_{18}-SCX multi-StageTip, a small portion of Empore Cation-SR Disk (3 M Company, St. Paul, MN) and C_{18} Disk, one disk per 10 μg of protein, were laminated in multiple in ordinary pipet tips. The StageTip was washed with 100% methanol, 80% ACN + 0.1% TFA, 2% ACN + 0.1%TFA, 500 mM ammonium bicarbonate + 30% ACN + 0.1% TFA, 2% ACN + 0.1% TFA, 80% ACN + 0.1% TFA, and 2% ACN + 0.1% TFA again. A pretreated plasma sample with Affi-Gel Blue and ACN precipitation was loaded onto the C_{18}-SCX multi-StageTip and washed with 2% ACN + 0.1% TFA. Then, APL1β peptides were eluted from the C_{18} disk with 120 μL of 80% ACN + 0.1% TFA to transfer to a cation-exchange disk. The StageTip was washed with 2% ACN + 0.1% TFA and 10 mM ammonium bicarbonate + 30% ACN + 0.1% TFA, and then APL1β peptides were eluted with 120 μL of 20 mM ammonium bicarbonate + 30% ACN + 0.1% TFA. The eluate was dried with a SpeedVac and resuspended in 25 μL of 20% acetonitrile and 0.1% TFA, and then 20 μL was analyzed with LC-MS/MS.

Setting of SRM/MRM Transition

SRM/MRM analysis was performed as previously described.[30] First, the mixture of endogenous and SI APL1β peptides was analyzed by LC-MS/MS using LTQ-Orbitrap Velos to acquire MS and MS/MS data (Supporting Information Figure 1). A preliminary SRM/MRM transition list for the peptides was

created from this acquired MS data using Pinpoint ver.1.0 (Thermo Fisher Scientific, Bremen, Germany). Then, the APL1β peptide mixture was analyzed using a TSQ-Vantage triple quadruple mass spectrometer (Thermo Fisher Scientific) with a nano-LC interface (AMR, Tokyo, Japan), Paradigm MS2 (Michrom Bioresources, Auburn, CA) and HTC PAL autosampler (CTC Analytics, Zwingen, Switzerland). The obtained data were analyzed using Pinpoint software to optimize parameters such as the collision energy (CE) and to acquire the retention times of each APL1β peptide. Finally, optimal transitions per peptide were selected for quantitation using SRM/MRM analysis (Table 1, Figure 2).

For the quantitation of plasma APL1β peptides by SRM/MRM, pretreated plasma dissolved in 20% acetonitrile and 0.1% TFA was analyzed by the above-mentioned optimal-timed SRM/MRM using TSQ-Vantage. SI peptide mixture was added to the pretreated samples at 5 fmol/mL, and endogenous peptides were quantified against spiked internal standard SI peptides. The flow rate of nanoLC was 500 nL/min and a linear gradient of ACN concentration was developed from 5 to 55% in several time windows, as indicated in the text and Figure 3. A spray voltage of 1900 V was applied. Data were acquired in nontime-scheduled SRM/MRM mode.

Data Analysis

APL1β peptides were quantitated using Pinpoint software. The peak area in the chromatogram of each SRM/MRM transition was measured and the amount of targeted peptides was calculated based on the peak area of the corresponding internal standard peptides. Final concentration of target peptides was determined as the average of all SRM/MRM transitions. The limits of detection (LODs) and quantification (LOQs) were determined as previously reported.[31]

RESULTS

Synthesis of Stable Isotope-Labeled Internal Standards APL1β peptides and Development of Transitions for SRM/MRM Analysis

For accurate quantitation of target peptides with SRM/MRM, stable isotope-labeled peptides (SI peptides) were used as internal standards. Thus, we synthesized nonlabeled and SI peptides for APL1β 25, 27, 28. The chemical purity of these peptides was more than 98% determined by RP-HPLC and/or by capillary zone electrophoresis. The exact quantities of the synthetic peptides were determined by amino acid analysis of their acid hydrolysates in order to apply them for absolute quantitation of APL1β peptides in human plasma. Also, full MS/MS spectra were obtained for sequence confirmation (Supporting Information Figure 1). Next, the SRM/MRM transitions and collision energy (CE) were generated for each targeted peptide (Table 1). The SI peptide standards were subsequently analyzed by monitoring the selected transitions, and visual inspection of the SRM/MRM transition peak was performed (Figure 1).

Depletion of Plasma Proteins and Unnecessary Peptides by Combination of Affi-Gel Blue, ACN Precipitation, and Multi-StageTips

For detection of low abundant plasma proteins by mass spectrometry, proteins need to be digested with proteases such as trypsin after enrichment of target proteins. However, tryptic digestion is not necessary to detect low abundant endogenous

Table 1. List of Transitions for SRM/MRM Analysis of APL1β Peptides

		endogenous						SI					
peptide	sequence	parent ion (m/z)	ion charge state	fragment ion (m/z)	ion charge state	ion type	CE	parent ion (m/z)	fragment ion (m/z)	ion charge state	ion type	CE
APL1β-25	DELAPAGTGVSREAVSGLLIMGAGG	776.734	3	969.020	2	b20	40	779.073	972.529	2	b20	41
				912.478	2	b19	40		915.987	2	b19	41
				392.159	1	y5	40		392.159	1	y5	41
				950.500	2	y21	40		950.500	2	y21	41
APL1β-27	DELAPAGTGVSREAVSGLLIMGAGGGS	824.751	3	969.020	2	b20	45	827.091	972.529	2	b20	45
				1022.528	2	y23	45		1022.528	2	y23	45
				912.478	2	b19	45		915.9868	2	b19	45
				1034.540	2	b21	45		1038.040	2	b21	45
APL1β-28	DELAPAGTGVSREAVSGLLIMGAGGGSL	862.446	3	912.478	2	b19	49	864.785	915.987	2	b19	49
				969.020	2	b20	49		972.529	2	b20	49
				1034.541	2	b21	48		1038.049	2	b21	48

dx.doi.org/10.1021/pr4010103 | J. Proteome Res. 2014, 13, 1012−1020

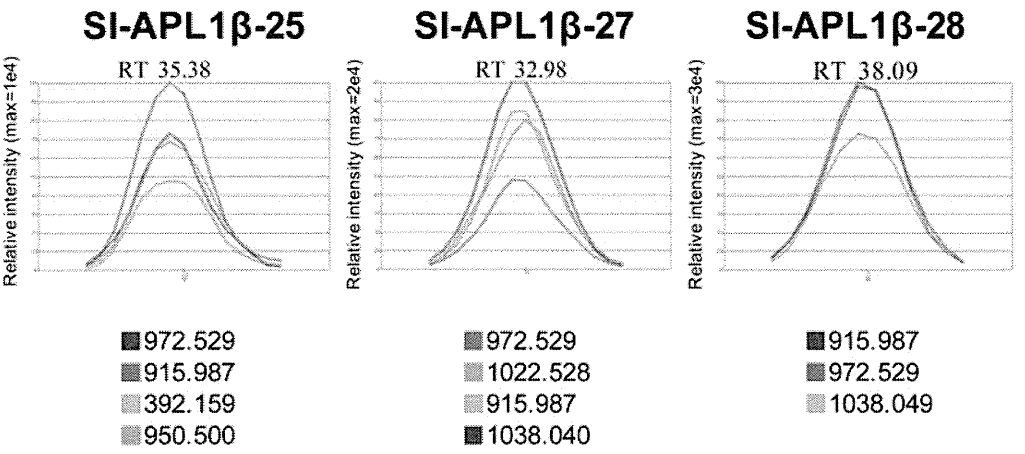

Figure 1. Peak shapes of selected transitions of SI APL1β peptides. See Table 1 for details of peptides. Retention time is shown as RT.

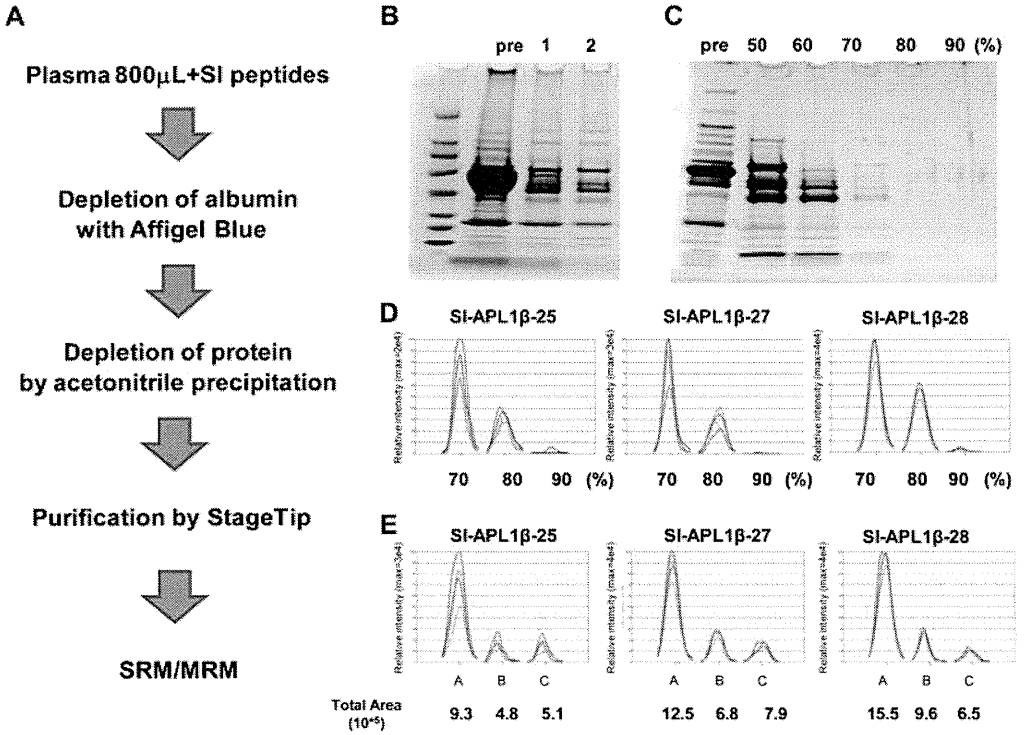

Figure 2. Depletion of plasma proteins and unnecessary peptides by combination of Affi-Gel Blue, ACN precipitation. and multi-StageTips. (A) Outline of the experimental workflow. (B) Depletion of plasma albumin using Affi-Gel Blue: pre, before depletion; 1, Affi-Gel Blue treatment once; 2, Affi-Gel Blue treatment twice. (C) Depletion of plasma proteins by different concentrations (50−90%) of acetonitrile precipitation: pre, untreated crude plasma. SDS-PAGE corresponding 0.02 μL plasma showed that most plasma proteins were depleted by >70% acetonitrile concentration. (D) Transition peaks of SI APL1β peptides spiked at the concentration of 5 fmol/mL after different concentrations (70−90%) of acetonitrile precipitation. Peak intensities were highest in the supernatant with 70% ACN precipitation and gradually decreased as ACN concentration increased. (E) Transition peaks of SI APL1β peptides spiked at the concentration of 5 fmol/mL after different plasma protein depletion methods. A: Combination of Affi-Gel Blue and ACN precipitation followed by StageTip purification. B: 70% ACN precipitation followed by StageTip purification. C: Ultrafiltration followed by StageTip purification. Total area of all transition peaks is shown. The combination of Affi-Gel Blue and ACN precipitation showed highest peak areas among the methods examined.

plasma peptides. Instead, removal of as much plasma proteins as possible is crucial.

To deplete most of the plasma proteins and enrich peptides efficiently, we used several methods. First, we tried 70% ACN precipitation or ultrafiltration (50 kDa MWCO) for depletion of plasma proteins and simultaneous recovery of APL1β peptides. The amount of APL1β peptides quantitated by SRM/MRM was lower after depletion of plasma proteins with 70% ACN precipitation and ultrafiltration as compared with combination with Affi-Gel Blue and ACN precipitation (data shown in Figure 2E), probably because APL1β peptides were captured with depleted or precipitated plasma proteins. Thus, we first depleted the most abundant plasma protein, albumin, with Cibacron Blue F3GA dye and subsequently depleted

residual plasma proteins with 70% ACN (Figure 2A). Eight hundred microliters of plasma diluted with an equal volume of Affi-Gel Blue depletion buffer were subjected to Affi-Gel Blue. The Coomassie Blue stained band corresponding to albumin in SDS-PAGE gel was almost abolished by two rounds of Affi-Gel Blue treatments (Figure 2B). Subsequently, ACN was added to the flow through to a final concentration of 50–90% and centrifuged to precipitate proteins. The supernatant was dried with SpeedVac and resuspended in 200 μL of 20% ACN and 0.1% TFA. SDS-PAGE analysis of the supernatant showed residual Coomassie Blue-stained bands in the supernatant of 50 and 60% ACN precipitation, whereas faint bands in the supernatant of >70% ACN precipitation (Figure 2C).

Unnecessary proteins/peptides were further depleted by passing through multi-StageTips containing reversed phase and cation-exchange materials. StageTips were developed by inserting Empore disks, chromatographic beads immobilized between Teflon meshworks, in an ordinary pipet tip.[29] Multi-StageTips were made by placing a combination of disks containing beads with different surfaces, which enabled 2D fractionation. We used C_{18}-SCX multi-StageTips to enrich APL1β peptides by organic solvent-based and strong cation fractionation. APL1β peptides bound to the StageTip were eluted with 20 mM ammonium bicarbonate, 30% ACN and 0.1% TFA, dried with SpeedVac, resuspended in 20% ACN and 0.1% TFA, and analyzed by SRM/MRM.

We examined peak areas of SI APL1β peptides spiked at the concentration of 5fmol/mL after treatment with ACN precipitation followed by StageTip purification. The peak areas were highest in the supernatant of 70% ACN precipitation and thus we decided to precipitate with 70% ACN (Figure 2D).

To investigate the recovery of APL1β peptides using different peptide enrichment procedures, we compared peak areas of SI APL1β peptides after the combination of Affi-Gel Blue and ACN precipitation with those treated with 70% ACN precipitation and ultrafiltration. As expected, peak areas of SI APL1β peptides using the combination of Affi-Gel Blue and ACN precipitation were 1.61–1.94 times and 1.58–2.38 times higher than 70% ACN precipitation and ultrafiltration, respectively (Figure 2E).

Evaluation of Recovery Efficiency of Plasma APL1β Peptides in the Sample Preparation Procedure

Recovery efficiency of plasma APL1β peptides in the sample preparation is crucial for the sensitivity of the assay. Thus, we assessed the recovery efficiency of plasma APL1β at each step of the workflow using SI peptides. The recovery was determined by measuring the relative amount of SI APL1β peptides before and after each step of the workflow. SI peptides were spiked into plasma, Affi-Gel Blue treated sample, Affi-Gel Blue treated and 70% ACN-precipitated sample, and the sample after StageTip purification at the concentration of 1 fmol/mL. Then, the relative peak area ratio of SI peptides before and after each step was compared to estimate the recovery efficiency. Recovery rates of APL1β peptides ranged from 71.7 to 86.0% after Affi-Gel Blue treatment, 69.3–83.4% after Affi-Gel Blue treatment and 70% ACN precipitation, and 50.2–64.0% after the overall procedure (Table 2).

Optimization of LC Gradient

SRM/MRM with SI internal standards peptides is a highly accurate quantitative method for peptides; however, problems with coeluting interference frequently occur. The key factors contributing to interference are the components of highly complex samples, such as plasma, referred to as biological "noise". To eliminate biological interference, we extended the separation time of LC, a gradient from 5% to 55% of ACN, from 20 to 120 min and examined the effect on interference. Supporting Information Figure 2 shows an example. Strikingly, a single peak observed with 20-min separation became a double peak when the separation time was extended to >40 min and the peak observed later was identified as a background peak of the sample. Thus, extension of the LC separation time was very effective to eliminate biological interference.

To shorten the total separation time of LC, we increased the gradient rapidly from 5% to 15% in one minute and then slowly from 15% to 30% in 35 min. The peak areas of APL1β peptides were comparable with those using 120-min separation (data not shown). Thus, we used the above LC separation method for the following experiments.

Table 2. Recovery Efficiency of Plasma APL1β Peptides in the Sample Preparation Procedure

	before	Affi-Gel Blue	Affi-Gel Blue ACN precipitation	Affi-Gel Blue ACN precipitation Stage-Tip
APL1β-25	100.00%	77.40%	76.90%	64.00%
APL1β-27	100.00%	71.70%	69.30%	50.20%
APL1β-28	100.00%	86.00%	83.40%	54.60%

LODs and LOQs of APL1β Peptides in Human Plasma

To examine the performance of our SRM/MRM assay, we evaluated the linear range, limits of detection (LODs), and quantitation (LOQs). The target SI peptides were spiked into 800 μL human plasma at nine different concentrations from 0 to 10 fmol, while nonlabeled synthetic peptides were spiked at a concentration of 10 fmol/mL in each sample as an internal standard. The concentration of target SI peptides at each concentration point was calculated based on the peak area of the corresponding internal standard peptides and determined as the average of all SRM/MRM transitions. Technical replicates were performed in triplicate at the nine concentration points. The linear correlation between the peak area ratios of the spiked SI peptides was obtained for each transition monitored over the 3 orders of magnitude, spanning peptide concentrations of 0.075–10 fmol/mL, measured in the experiment (R^2 > 0.99) (Figure 3), which indicates that the target peptides were able to be quantified without interference from the endogenous peptide or passenger peptide. This also allowed for the characterization of LODs and LOQs, which was determined as average blank measurements +3 and 10 times SD, respectively, calculated based on the peak area of nonlabeled internal standard peptides, as previously reported.[31] LODs and LOQs corresponding to APL1β differed between the transitions used and were 0.095–0.227 and 0.237–0.632 fmol/mL for APL1β 25, 0.131–0.278 and 0.318–0.734 fmol/mL for APL1β 27, and 0.076–0.162 and 0.152–0.342 fmol/mL for APL1β 28 (Table 3). Importantly, coefficients of variance (CVs) of the peak area between measurements (n = 3) often fell below 20% under the LOQ level (Figure 3). Schoenherr et al. used the lowest points above LOD with CV < 20% as LOQ.[32] Thus, we also defined LOQ as the lowest point of the spiked APL1β 25, 27, 28 peptides with CV < 20% between measurements above LOD, which was 0.3 fmol/mL (<1 pg/mL) (Figure 3). This LOQ was much lower than that of previously reported plasma gastric inhibitory polypeptide quantitation (1–10 fmol/mL).[28]

dx.doi.org/10.1021/pr4010103 | J. Proteome Res. 2014, 13, 1012–1020

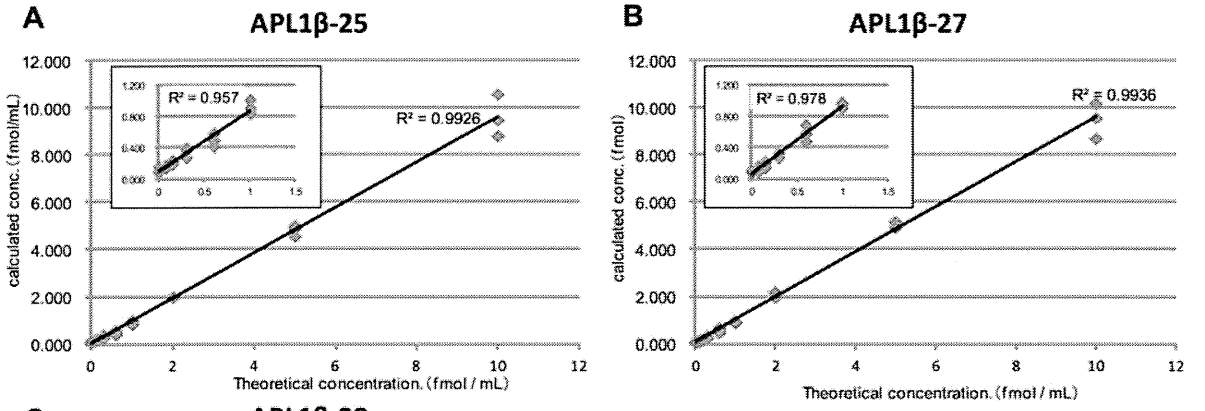

D

APL1β-25	0 (fmol/mL)	0.075 (fmol/mL)	0.15 (fmol/mL)	0.3 (fmol/mL)	0.6 (fmol/mL)	1.0 (fmol/mL)	2.0 (fmol/mL)	5.0 (fmol/mL)	10.0 (fmol/mL)
Mean (fmol/mL)	0.107	0.144	0.209	0.334	0.485	0.908	1.986	4.81	9.625
SD	0.036	0.012	0.023	0.061	0.08	0.084	0.002	0.226	0.90
CV(%)	33.3	8.4	11.2	18.2	16.5	9.3	0.1	4.7	9.3

APL1β-27	0 (fmol/mL)	0.075 (fmol/mL)	0.15 (fmol/mL)	0.3 (fmol/mL)	0.6 (fmol/mL)	1.0 (fmol/mL)	2.0 (fmol/mL)	5.0 (fmol/mL)	10.0 (fmol/mL)
Mean (fmol/mL)	0.088	0.115	0.174	0.285	0.573	0.933	2.104	5.091	9.485
SD	0.011	0.029	0.035	0.03	0.103	0.036	0.112	0.139	0.755
CV(%)	12.0	25.3	20.1	10.6	18.0	3.9	5.3	2.7	8.0

APL1β-28	0 (fmol/mL)	0.075 (fmol/mL)	0.15 (fmol/mL)	0.3 (fmol/mL)	0.6 (fmol/mL)	1.0 (fmol/mL)	2.0 (fmol/mL)	5.0 (fmol/mL)	10.0 (fmol/mL)
Mean (fmol/mL)	0.081	0.107	0.149	0.283	0.514	1.013	1.951	5.141	10.579
SD	0.038	0.025	0.036	0.054	0.094	0.13	0.103	0.158	0.20
CV(%)	46.9	23.2	23.9	19.2	18.2	12.8	5.3	3.1	1.9

Figure 3. Calibration curve and CV of the peak area. Target SI APL1β 25 (A), 27 (B), and 28 (C) peptides were spiked into 800 μL human plasma at concentrations of 0, 0.075, 0.15, 0.3, 0.6, 1, 2, 5, 10 fmol/mL and 0.075, 0.15, 0.3, 0.6, 1 fmol/mL (insets). Concentrations of the spiked SI peptides were calculated using the peak area of spiked nonlabeled synthetic peptides at the concentration of 10 fmol/mL and determined as the average of all SRM/MRM transitions. Mean, SD, and CV from triplicate experiments are shown in (D). The linear correlations between the peak area ratios of the spiked SI peptides were obtained for each transition monitored over 3 orders of magnitude, spanning peptide concentrations of 0.075–10 fmol/mL, measured in the experiment ($R^2 > 0.99$).

Table 3. LODs and LOQs of APL1β Peptides

		transition			
peptide	sequence	parent ion (m/z)	fragment ion (m/z)	LOD (fmol/mL)	LOQ (fmol/mL)
APL1β-25	DELAPAGTGVSREAVSGLLIMGAGG	779.073	972.529	0.095	0.237
			915.987	0.129	0.316
			392.159	0.226	0.609
			950.500	0.227	0.632
APL1β-27	DELAPAGTGVSREAVSGLLIMGAGGGS	827.091	972.529	0.212	0.506
			1022.528	0.131	0.318
			915.987	0.278	0.734
			1038.040	0.257	0.675
APL1β-28	DELAPAGTGVSREAVSGLLIMGAGGGSL	864.785	915.987	0.099	0.282
			972.529	0.076	0.152
			1038.049	0.162	0.342

Absolute Quantitation of APL1β Peptides in Human Plasma

Next, we investigated the detection and quantification of endogenous APL1β peptides. The profile of the transition peaks of SI peptide and endogenous peptide was comparable (Supporting Information Figure 3), which qualified the transitions used for quantification. The concentration of endogenous APL1β was calculated based on the peak area of the corresponding SI peptides and determined as the average of all SRM/MRM transitions. Based on the peak area of the SI internal control peptides, absolute concentrations of APL1β25, 27, 28 peptides in plasma samples obtained from three healthy controls and two AD patients were quantified as shown in Figure 4A and B: healthy control, 0.638–0.796 fmol/mL for APL1β25, 0.4310.572 fmol/mL APL1β27, and 0.408–0.510 fmol/mL for APL1β28; AD patients, 0.517 and 0.609 fmol/mL

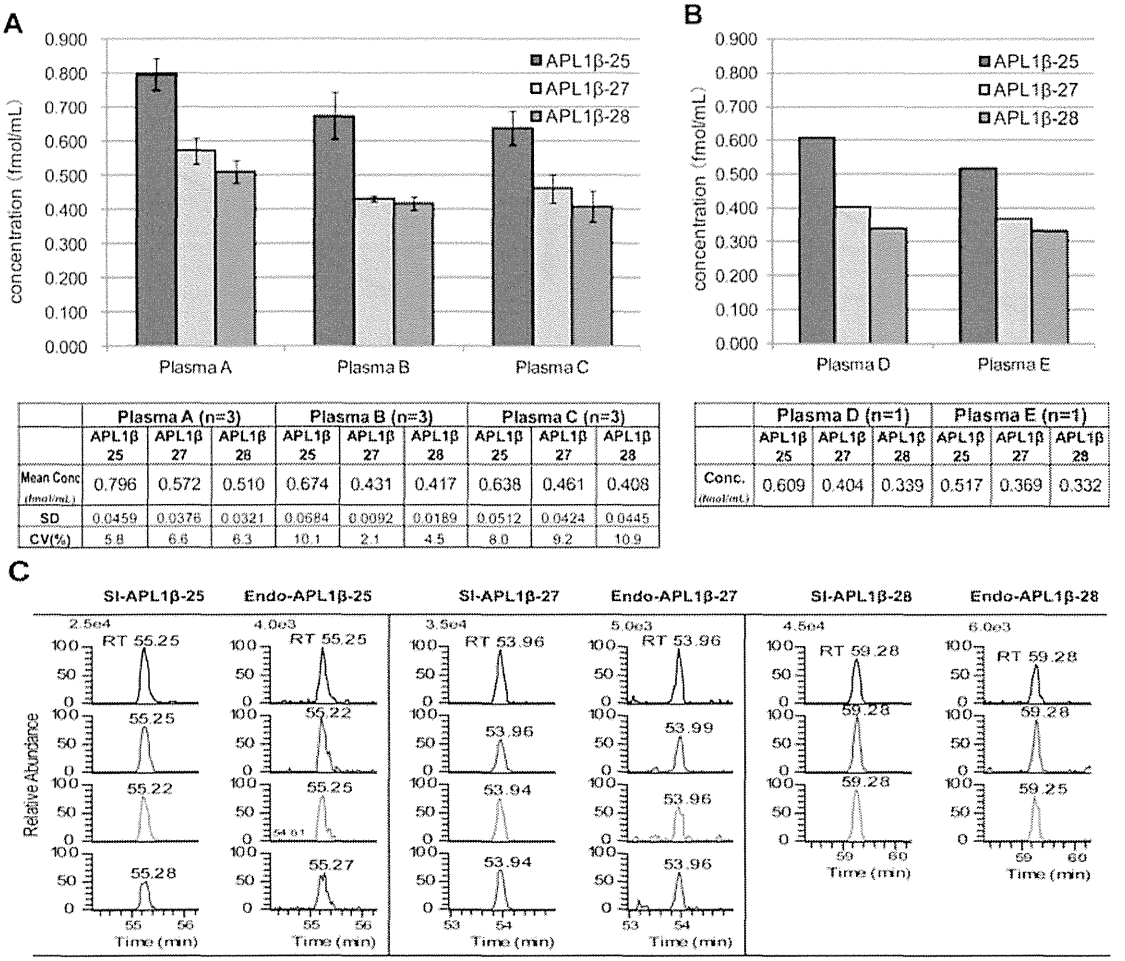

	Plasma A (n=3)			Plasma B (n=3)			Plasma C (n=3)		
	APL1β 25	APL1β 27	APL1β 28	APL1β 25	APL1β 27	APL1β 28	APL1β 25	APL1β 27	APL1β 28
Mean Conc (fmol/mL)	0.796	0.572	0.510	0.674	0.431	0.417	0.638	0.461	0.408
SD	0.0459	0.0376	0.0321	0.0684	0.0092	0.0189	0.0512	0.0424	0.0445
CV(%)	5.8	6.6	6.3	10.1	2.1	4.5	8.0	9.2	10.9

	Plasma D (n=1)			Plasma E (n=1)		
	APL1β 25	APL1β 27	APL1β 28	APL1β 25	APL1β 27	APL1β 28
Conc. (fmol/mL)	0.609	0.404	0.339	0.517	0.369	0.332

Figure 4. Absolute quantitation of APL1β peptides in human plasma. (A) Based on the peak area of the SI internal control peptides, absolute concentrations of APL1β25, 27, 28 peptides in plasma samples of three healthy controls were 0.638−0.796 fmol/mL for APL1β25, 0.431−0.572 fmol/mL for APL1β27, and 0.408−0.510 fmol/mL for APL1β28 (n = 3) with CV values of <11%. (B) Absolute concentrations of APL1β25, 27, 28 peptides in plasma samples of two AD patients were 0.517−0.609 fmol/mL for APL1β25, 0.369−0.404 fmol/mL for APL1β27, and 0.332−0.339 fmol/mL for APL1β28 (n = 1). (C) Extracted ion chromatograms of endogenous and SI APL1β peptides in a healthy control plasma.

for APL1β25, 0.369, and 0.404 fmol/mL APL1β27, and 0.332 and 0.339 fmol/mL for APL1β28, respectively. APL1β levels of AD patients were at the same level as that of the healthy control. Extracted ion chromatograms of endogenous and SI APL1β peptides in a healthy control plasma are shown in Figure 4C as an example. Notably, both endogenous and SI APL1β peptides showed a high signal-to-noise ratio. Moreover, all CV values between measurements of endogenous APL1β peptides were below 11% and those between transitions were below 25% (Figure 4A, Supporting Information Tables 1, 2).

DISCUSSION

In the present study, we succeeded in quantifying low abundant plasma surrogate marker peptides for AD, APL1β, using several preanalytical and analytical approaches without immunoaffinity enrichment. Plasma concentration of APL1β peptides was determined as several hundred amol/mL. This low level of endogenous peptides has not been reported previously. Our approach would be widely applicable for targeted proteomics to quantify low abundant peptides of interest in complex biological samples.

Enrichment of proteins using antibodies is a common approach to detect and quantify low abundant proteins.[9−12] However, immunoprecipitation of proteins of interest is quite labor intensive and highly expensive. In contrast, if the analytes of interest are small molecules, such as peptides in biofluids, removal of proteins can eliminate a huge potential source of interference in mass spectrometric analysis. Several methods have been reported to deplete proteins in biofluids, such as ultrafiltration, organic precipitation, or an immunodepletion column before analysis;[22−25] however, the most suitable preanalytical method will depend on the peptides of interest. In this study, APL1β peptides were hardly detected by SRM/MRM after ultrafiltration (50 kDa MWCO) or ACN precipitation alone. This is probably because APL1β peptides were also depleted with plasma proteins, especially with albumin, possibly due to the hydrophobic nature of the peptides. To solve this problem, we performed two-step plasma depletion, which consists of the removal of albumin using Affi-Gel Blue followed by ACN precipitation. Albumin was depleted in a buffer containing a surfactant, n-octyl-β-glucoside, which might be able to remove low molecular weight peptides bound to albumin.

Even if plasma proteins are depleted, a number of different peptides exist in the resulting sample that interfere with the detection of the target peptides. StageTips are ordinary pipet tips containing very small disks made of beads with reversed-phase, cation-exchange, or anion-exchange surfaces embedded in Teflon mesh.[29] Disks with different surfaces can be combined to make multi-StageTips that enable 2D fractionation. In this study, unnecessary peptides could be depleted by the combination of reversed-phase and cation-exchange surfaces, which would help to yield high sensitivity for the detection of APL1β peptides.

The resolving power of LC separation is directly proportional to the total gradient time. Using a long gradient with a slow increase in ACN concentration, better separation of peptides with similar polarity may be achieved. However, this will occur with a loss of signal intensity as the width of the peak increases. In this study, we observed small molecules that have both a precursor mass and fragment ion masses that are nearly identical to those of APL1β peptides that cause transition interference. Extending the gradient time enabled the separation of small molecules from APL1β peptides to avoid interference.

In conclusion, APL1β peptides were able to be quantified as several hundred amol/mL by SRM/MRM without immunoaffinity enrichment of the peptides. Our method would be useful in clinical applications to quantitate any low abundant plasma peptide biomarkers.

■ ASSOCIATED CONTENT

Supporting Information

Supplementary Figure 1: MS and MS/MS data of APL1β peptides. Supplementary Figure 2. Optimization of LC gradient. Supplementary Figure 3: Transition peak profiles of endogenous and SI APL1β peptides in plasma samples. Supplementary Table 1: Quantitation data of endogenous APL1β peptides in plasma samples of healthy controls. Supplementary Table 2: Quantitation data of endogenous APL1β peptides in plasma samples of AD patients. This material is available free of charge via the Internet at http://pubs.acs.org.

■ AUTHOR INFORMATION

Corresponding Author

*E-mail: tomonaga@nibio.go.jp. Tel.: +81-72-641-9862. Fax: +81-72-641-9861.

Notes

The authors declare no competing financial interest.

■ ACKNOWLEDGMENTS

This work was the result of "Integrated Research on Neuropsychiatric Disorders" carried out under the Strategic Research Program for Brain Sciences by the Ministry of Education, Culture, Sports, Science and Technology and "Research on Biological Markers for New Drug Development H20-0005" by the Ministry of Health, Labour and Welfare of Japan.

■ ABBREVIATIONS

SRM/MRM, selected/multiple reaction monitoring; APL1β, APLP1-derived Aβ-like peptides; LC–MS/MS, liquid chromatography tandem mass spectrometry; SI, stable isotope labeled; ACN, acetonitrile; SCX, strong cation-exchange; TFA, trifluoroacetic acid; CE, collision energy; LTQ, linear ion trap; LOQs, limits of quantification; CV, coefficient of variance

■ REFERENCES

(1) Lange, V.; Picotti, P.; Domon, B.; Aebersold, R. Selected reaction monitoring for quantitative proteomics: a tutorial. *Mol. Syst. Biol.* **2008**, *4*, 222.

(2) Kuhn, E.; Wu, J.; Karl, J.; Liao, H.; Zolg, W.; Guild, B. Quantification of C-reactive protein in the serum of patients with rheumatoid arthritis using multiple reaction monitoring mass spectrometry and 13C-labeled peptide standards. *Proteomics* **2004**, *4* (4), 1175–86.

(3) Anderson, L.; Hunter, C. L. Quantitative mass spectrometric multiple reaction monitoring assays for major plasma proteins. *Mol. Cell. Proteomics* **2006**, *5* (4), 573–88.

(4) Keshishian, H.; Addona, T.; Burgess, M.; Kuhn, E.; Carr, S. A. Quantitative, multiplexed assays for low abundance proteins in plasma by targeted mass spectrometry and stable isotope dilution. *Mol. Cell. Proteomics* **2007**, *6* (12), 2212–29.

(5) Keshishian, H.; Addona, T.; Burgess, M.; Mani, D. R.; Shi, X.; Kuhn, E.; Sabatine, M. S.; Gerszten, R. E.; Carr, S. A. Quantification of cardiovascular biomarkers in patient plasma by targeted mass spectrometry and stable isotope dilution. *Mol. Cell. Proteomics* **2009**, *8* (10), 2339–49.

(6) Liu, T.; Qian, W. J.; Mottaz, H. M.; Gritsenko, M. A.; Norbeck, A. D.; Moore, R. J.; Purvine, S. O.; Camp, D. G., 2nd; Smith, R. D. Evaluation of multiprotein immunoaffinity subtraction for plasma proteomics and candidate biomarker discovery using mass spectrometry. *Mol. Cell. Proteomics* **2006**, *5* (11), 2167–74.

(7) Qian, W. J.; Kaleta, D. T.; Petritis, B. O.; Jiang, H.; Liu, T.; Zhang, X.; Mottaz, H. M.; Varnum, S. M.; Camp, D. G., 2nd; Huang, L.; Fang, X.; Zhang, W. W.; Smith, R. D. Enhanced detection of low abundance human plasma proteins using a tandem IgY12-SuperMix immunoaffinity separation strategy. *Mol. Cell. Proteomics* **2008**, *7* (10), 1963–73.

(8) Anderson, N. L.; Anderson, N. G.; Haines, L. R.; Hardie, D. B.; Olafson, R. W.; Pearson, T. W. Mass spectrometric quantitation of peptides and proteins using Stable Isotope Standards and Capture by Anti-Peptide Antibodies (SISCAPA). *J. Proteome Res.* **2004**, *3* (2), 235–44.

(9) Whiteaker, J. R.; Zhao, L.; Zhang, H. Y.; Feng, L. C.; Piening, B. D.; Anderson, L.; Paulovich, A. G. Antibody-based enrichment of peptides on magnetic beads for mass-spectrometry-based quantification of serum biomarkers. *Anal. Biochem.* **2007**, *362* (1), 44–54.

(10) Kuhn, E.; Addona, T.; Keshishian, H.; Burgess, M.; Mani, D. R.; Lee, R. T.; Sabatine, M. S.; Gerszten, R. E.; Carr, S. A. Developing multiplexed assays for troponin I and interleukin-33 in plasma by peptide immunoaffinity enrichment and targeted mass spectrometry. *Clin. Chem.* **2009**, *55* (6), 1108–17.

(11) Whiteaker, J. R.; Zhao, L.; Anderson, L.; Paulovich, A. G. An automated and multiplexed method for high throughput peptide immunoaffinity enrichment and multiple reaction monitoring mass spectrometry-based quantification of protein biomarkers. *Mol. Cell. Proteomics* **2010**, *9* (1), 184–96.

(12) Whiteaker, J. R.; Zhao, L.; Abbatiello, S. E.; Burgess, M.; Kuhn, E.; Lin, C.; Pope, M. E.; Razavi, M.; Anderson, N. L.; Pearson, T. W.; Carr, S. A.; Paulovich, A. G. Evaluation of large scale quantitative proteomic assay development using peptide affinity-based mass spectrometry. *Mol. Cell. Proteomics* **2011**, M110.005645.

(13) Lopez, M. F.; Rezai, T.; Sarracino, D. A.; Prakash, A.; Krastins, B.; Athanas, M.; Singh, R. J.; Barnidge, D. R.; Oran, P.; Borges, C.; Nelson, R. W. Selected reaction monitoring-mass spectrometric immunoassay responsive to parathyroid hormone and related variants. *Clin. Chem.* **2010**, *56* (2), 281–90.

(14) Shi, T.; Fillmore, T. L.; Sun, X.; Zhao, R.; Schepmoes, A. A.; Hossain, M.; Xie, F.; Wu, S.; Kim, J. S.; Jones, N.; Moore, R. J.; Pasa-Tolic, L.; Kagan, J.; Rodland, K. D.; Liu, T.; Tang, K.; Camp, D. G.,

2nd; Smith, R. D.; Qian, W. J. Antibody-free, targeted mass-spectrometric approach for quantification of proteins at low picogram per milliliter levels in human plasma/serum. *Proc. Natl. Acad. Sci. U.S.A.* **2012**, *109* (38), 15395–400.
(15) Masters, C. L.; Simms, G.; Weinman, N. A.; Multhaup, G.; McDonald, B. L.; Beyreuther, K. Amyloid plaque core protein in Alzheimer disease and Down syndrome. *Proc. Natl. Acad. Sci. U.S.A.* **1985**, *82* (12), 4245–9.
(16) Selkoe, D. J. Alzheimer's disease: genes, proteins, and therapy. *Physiol. Rev.* **2001**, *81* (2), 741–66.
(17) Andreasen, N.; Hesse, C.; Davidsson, P.; Minthon, L.; Wallin, A.; Winblad, B.; Vanderstichele, H.; Vanmechelen, E.; Blennow, K. Cerebrospinal fluid beta-amyloid(1–42) in Alzheimer disease: differences between early- and late-onset Alzheimer disease and stability during the course of disease. *Arch. Neurol.* **1999**, *56* (6), 673–80.
(18) Jensen, M.; Schroder, J.; Blomberg, M.; Engvall, B.; Pantel, J.; Ida, N.; Basun, H.; Wahlund, L. O.; Werle, E.; Jauss, M.; Beyreuther, K.; Lannfelt, L.; Hartmann, T. Cerebrospinal fluid A beta42 is increased early in sporadic Alzheimer's disease and declines with disease progression. *Ann. Neurol.* **1999**, *45* (4), 504–11.
(19) Motter, R.; Vigo-Pelfrey, C.; Kholodenko, D.; Barbour, R.; Johnson-Wood, K.; Galasko, D.; Chang, L.; Miller, B.; Clark, C.; Green, R.; et al. Reduction of beta-amyloid peptide42 in the cerebrospinal fluid of patients with Alzheimer's disease. *Ann. Neurol.* **1995**, *38* (4), 643–8.
(20) Okochi, M.; Steiner, H.; Fukumori, A.; Tanii, H.; Tomita, T.; Tanaka, T.; Iwatsubo, T.; Kudo, T.; Takeda, M.; Haass, C. Presenilins mediate a dual intramembranous gamma-secretase cleavage of Notch-1. *EMBO J.* **2002**, *21* (20), 5408–16.
(21) Yanagida, K.; Okochi, M.; Tagami, S.; Nakayama, T.; Kodama, T. S.; Nishitomi, K.; Jiang, J.; Mori, K.; Tatsumi, S.; Arai, T.; Ikeuchi, T.; Kasuga, K.; Tokuda, T.; Kondo, M.; Ikeda, M.; Deguchi, K.; Kazui, H.; Tanaka, T.; Morihara, T.; Hashimoto, R.; Kudo, T.; Steiner, H.; Haass, C.; Tsuchiya, K.; Akiyama, H.; Kuwano, R.; Takeda, M. The 28-amino acid form of an APLP1-derived Abeta-like peptide is a surrogate marker for Abeta42 production in the central nervous system. *EMBO Mol. Med.* **2009**, *1* (4), 223–35.
(22) Zheng, X.; Baker, H.; Hancock, W. S. Analysis of the low molecular weight serum peptidome using ultrafiltration and a hybrid ion trap-Fourier transform mass spectrometer. *J. Chromatogr. A* **2006**, *1120* (1–2), 173–84.
(23) Tammen, H.; Schulte, I.; Hess, R.; Menzel, C.; Kellmann, M.; Mohring, T.; Schulz-Knappe, P. Peptidomic analysis of human blood specimens: comparison between plasma specimens and serum by differential peptide display. *Proteomics* **2005**, *5* (13), 3414–22.
(24) Kay, R.; Barton, C.; Ratcliffe, L.; Matharoo-Ball, B.; Brown, P.; Roberts, J.; Teale, P.; Creaser, C. Enrichment of low molecular weight serum proteins using acetonitrile precipitation for mass spectrometry based proteomic analysis. *Rapid Commun. Mass Spectrom.* **2008**, *22* (20), 3255–60.
(25) Aristoteli, L. P.; Molloy, M. P.; Baker, M. S. Evaluation of endogenous plasma peptide extraction methods for mass spectrometric biomarker discovery. *J. Proteome Res.* **2007**, *6* (2), 571–81.
(26) Chambers, E. E.; Lame, M. E.; Bardsley, J.; Hannam, S.; Legido-Quigley, C.; Smith, N.; Fountain, K. J.; Collins, E.; Thomas, E. High sensitivity LC-MS/MS method for direct quantification of human parathyroid 1–34 (teriparatide) in human plasma. *J. Chromatogr. B: Anal. Technol. Biomed. Life Sci.* **2013**, *938*, 96–104.
(27) Chen, Z.; Caulfield, M. P.; McPhaul, M. J.; Reitz, R. E.; Taylor, S. W.; Clarke, N. J. Quantitative insulin analysis using liquid chromatography-tandem mass spectrometry in a high-throughput clinical laboratory. *Clin. Chem.* **2013**, *59* (9), 1349–56.
(28) Miyachi, A.; Murase, T.; Yamada, Y.; Osonoi, T.; Harada, K. Quantitative analytical method for determining the levels of gastric inhibitory polypeptides GIP1–42 and GIP3–42 in human plasma using LC-MS/MS/MS. *J. Proteome Res.* **2013**, *12* (6), 2690–9.
(29) Rappsilber, J.; Mann, M.; Ishihama, Y. Protocol for micro-purification, enrichment, pre-fractionation and storage of peptides for proteomics using StageTips. *Nat. Protoc.* **2007**, *2* (8), 1896–906.
(30) Muraoka, S.; Kume, H.; Watanabe, S.; Adachi, J.; Kuwano, M.; Sato, M.; Kawasaki, N.; Kodera, Y.; Ishitobi, M.; Inaji, H.; Miyamoto, Y.; Kato, K.; Tomonaga, T. Strategy for SRM-based verification of biomarker candidates discovered by iTRAQ method in limited breast cancer tissue samples. *J. Proteome Res.* **2012**, *11* (8), 4201–10.
(31) Whiteaker, J. R.; Lin, C.; Kennedy, J.; Hou, L.; Trute, M.; Sokal, I.; Yan, P.; Schoenherr, R. M.; Zhao, L.; Voytovich, U. J.; Kelly-Spratt, K. S.; Krasnoselsky, A.; Gafken, P. R.; Hogan, J. M.; Jones, L. A.; Wang, P.; Amon, L.; Chodosh, L. A.; Nelson, P. S.; McIntosh, M. W.; Kemp, C. J.; Paulovich, A. G. A targeted proteomics-based pipeline for verification of biomarkers in plasma. *Nat. Biotechnol.* **2011**, *29* (7), 625–34.
(32) Schoenherr, R. M.; Whiteaker, J. R.; Zhao, L.; Ivey, R. G.; Trute, M.; Kennedy, J.; Voytovich, U. J.; Yan, P.; Lin, C.; Paulovich, A. G. Multiplexed quantification of estrogen receptor and HER2/Neu in tissue and cell lysates by peptide immunoaffinity enrichment mass spectrometry. *Proteomics* **2012**, *12* (8), 1253–60.

Selective evaluation of high density lipoprotein from mouse small intestine by an in situ perfusion technique[S]

Satoshi Yamaguchi,[1,*] Bo Zhang,[1,†] Takeshi Tomonaga,[§] Utako Seino,[**] Akiko Kanagawa,[§] Masaru Segawa,[††] Hironori Nagasaka,[§§] Akira Suzuki,[*] Takashi Miida,[***] Sohsuke Yamada,[†††] Yasuyuki Sasaguri,[†††] Takefumi Doi,[§§§] Keijiro Saku,[****] Mitsuyo Okazaki,[††††] Yoshihiro Tochino,[§§§§] and Ken-ichi Hirano[2,*]

Laboratory of Cardiovascular Disease,* Novel, Non-invasive and Nutritional Therapeutics (CNT), Graduate School of Medicine, Osaka University, Osaka, Japan; Department of Biochemistry,[†] Fukuoka University School of Medicine, Fukuoka, Japan; Laboratory of Proteome Research,[§] National Institute of Biomedical Innovation, Osaka, Japan; Niigata Prefectural Institute of Environmental Radiation Monitoring,** Niigata Branch, Niigata, Japan; Central Laboratory for Pathology and Morphology,[††] Fukuoka University School of Medicine, Fukuoka, Japan; Department of Pediatrics,[§§] Takarazuka City Hospital, Takarazuka, Japan; Department of Clinical Laboratory Medicine,*** Juntendo University School of Medicine, Tokyo, Japan; Department of Pathology and Cell Biology,[†††] School of Medicine, University of Occupational and Environmental Health, Kitakyushu, Japan; Graduate School of Pharmaceutical Sciences,[§§§] Osaka University, Osaka, Japan; Department of Cardiology,**** Fukuoka University School of Medicine, Fukuoka, Japan; Professor Emeritus of Tokyo Medical and Dental University,[††††] Skylight Biotech Inc., Akita, Japan; Department of Metabolic Medicine,[§§§§] Graduate School of Medicine, Osaka University, Osaka, Japan

Abstract The small intestine (SI) is the second-greatest source of HDL in mice. However, the selective evaluation of SI-derived HDL (SI-HDL) has been difficult because even the origin of HDL obtained in vivo from the intestinal lymph duct of anesthetized rodents is doubtful. To shed light on this question, we have developed a novel in situ perfusion technique using surgically isolated mouse SI, with which the possible filtration of plasma HDL into the SI lymph duct can be prevented. With the developed method, we studied the characteristics of and mechanism for the production and regulation of SI-HDL. Nascent HDL particles were detected in SI lymph perfusates in WT mice, but not in ABCA1 KO mice. SI-HDL had a high protein content and was smaller than plasma HDL. SI-HDL was rich in TG and apo AIV compared with HDL in liver perfusates. SI-HDL was increased by high-fat diets and reduced in apo E KO mice. In conclusion, with our in situ perfusion model that enables the selective evaluation of SI-HDL, we demonstrated that ABCA1 plays an important role in intestinal HDL production, and SI-HDL is small, dense, rich in apo AIV, and regulated by nutritional and genetic factors.—Yamaguchi, S., B. Zhang, T. Tomonaga, U. Seino, A. Kanagawa, M. Segawa, H. Nagasaka, A. Suzuki, T. Miida, S. Yamada, Y. Sasaguri, T. Doi, K. Saku, M. Okazaki, Y. Tochino, and K. Hirano. **Selective evaluation of high density lipoprotein from mouse small intestine by an in situ perfusion technique. *J. Lipid Res.* 2014.** 55: **905–918.**

Supplementary key words atherosclerosis • regulation • lipoprotein • in situ perfusion • intestine

HDL is unquestionably a major antiatherogenic factor worldwide, regardless of sex, race, and age (1, 2). Therefore, an increase in HDL levels has been an important goal that guides the development of novel therapies for atherosclerotic cardiovascular diseases (3) because it was reported that plasma HDL cholesterol (HDL-C) levels were reduced in patients with ischemic heart disease and stroke (4, 5). Strategies for raising HDL are now available. Because remarkable progress has been made in our understanding of the molecular mechanism of HDL production, enhanced production is one of the major strategies for raising HDL.

ABCA1, mutations of which are the genetic cause of Tangier disease and genetic HDL deficiency, is one of the

Abbreviations: ACN, acetonitrile; CE, cholesterol ester; CETP, cholesteryl ester transfer protein; C-HDL, HDL in mesenteric lymph obtained by conventional intestinal lymph cannulation experiments; CM, chylomicron; EM, electron microscopy; FC, free cholesterol; HDL-C, HDL cholesterol; L-HDL, HDL in liver perfusates; P-HDL, plasma HDL; PL, phospholipid; SI, small intestine; SI-HDL, small-intestine-derived HDL; TC, total cholesterol; TEM, transmission electron microscopy.

[1] S. Yamaguchi and B. Zhang contributed equally to this work.

[2] To whom correspondence should be addressed.

e-mail: khirano@cnt-osaka.com; khirano@cardiology.med.osaka-u.ac.jp

[S] The online version of this article (available at http://www.jlr.org) contains supplementary data in the form of two figures.

This study was partially supported by research grants-in-aid for rare and intractable diseases from the Ministry of Health, Labour, and Welfare of Japan, for Scientific Research (C) (23617010), grants-in-aid from the Ministry of Education, Culture, Sports, Science and Technology of Japan (No. 23590699), and grants for K. Hirano from Novartis Institutes for Biomedical Research Tsukuba (2005) and Shionogi and Co. Ltd. (FINDS2007).

Manuscript received 30 January 2014 and in revised form 25 February 2014.

Published, JLR Papers in Press, February 25, 2014
DOI 10.1194/jlr.M047761

prerequisite molecules for the production of HDL (6–8). We and others found that a human intestinal cell line, CaCo-2, expresses ABCA1 (9, 10) and secretes HDL though the involvement of ABCA1 (11). Experimental studies with rodents have demonstrated that the liver and small intestine (SI) are the major organs for ABCA1 expression and HDL production (12–16). Recent findings have shown that, although the overexpression of hepatic ABCA1 in experimental mouse models is not beneficial (17), the overexpression of intestinal ABCA1 is beneficial for atherosclerosis (18), indicating that HDL from SI may perform unique and distinct functions.

However, the characterization of SI-derived HDL (SI-HDL) and clarification of the mechanism that underlies its production and regulation remain elusive because selective evaluation of SI-HDL is difficult. Since the 1970s, various studies have demonstrated that HDL can be obtained from the intestinal lymph duct of anesthetized rodents in vivo, but its origin has been doubtful because it has been suggested that the source is either the secretion of HDL by the SI or the filtration of HDL from plasma through the blood capillary-lymph loop into the intestinal lymph duct (19–22).

In this regard, the group of Hayden et al. (16) recently reported the interesting and unexpected finding that HDL from the intestinal lymph duct was not reduced in SI-specific ABCA1 KO mice but was markedly reduced in liver-specific ABCA1 KO mice. The authors concluded that SI-HDL may be secreted directly into the circulation and that HDL in the intestinal lymph duct is predominantly derived from plasma. However, this conclusion is tenable only if a substantial quantity of plasma HDL, the majority of which is derived from the liver, passes through the loop and enters the intestinal lymph duct, so that the liver-specific disruption of ABCA1 affects the quantity of HDL obtained from the intestinal lymph duct more than does the SI-specific disruption of ABCA1.

To prevent the possible filtration of plasma HDL into the intestinal lymph duct and to realize the selective evaluation of SI-HDL, we developed an in situ perfusion technique using surgically isolated mouse SI. With this technique, we could demonstrate that the SI produces HDL, which reaches at least the SI lymph duct, and that the production of SI-HDL may be dynamically regulated.

METHODS

Animals

WT C57BL6/J mice, ABCA1 KO, and apo E KO mice were obtained from the Jackson Laboratory (Bar Harbor, ME) and housed in a room under controlled temperature and humidity conditions and with free access to water and chow. Experiments were conducted when the male mice were aged from 12 to 16 weeks. Blood was drawn for the measurement of plasma lipid levels by enzymatic methods. The experimental protocol was approved by the Ethics Review Committee for Animal Experimentation of Osaka University.

In situ perfusion system for the evaluation of HDL production in the SI

We developed an in situ perfusion model in mice with isolated SI in which the arterial blood supply for the SI has been blocked for the assessment of HDL production in mouse SI (**Fig. 1A** and supplementary Fig. I). This novel in situ perfusion model can be used for the evaluation of HDL originated from the SI without intrusion by the filtration of HDL from plasma. The detailed experimental procedures are available in the form of video upon request. After the mice were deeply anesthetized, the abdominal cavity was opened, and the appropriate arteries except for the abdominal aorta were ligated to block the blood supply for the SI (Fig. 1A). Argatroban was injected intravenously as an anticoagulant (23), and 5 min after injection, the mice were euthanized for the removal of tissues including the heart and lungs from the thorax, except for the thoracic descending aorta. At this point, the SI would become ischemic.

To protect the SI from organ damage, the following procedures needed to be performed quickly. Two tubes were inserted into the abdominal aorta and portal vein by the following procedure. First, a needle (26G) connected to a tube was inserted antegrade through the thoracic descending aorta into the abdominal aorta, which was then ligated with the needle inserted at distal to the inserted portion to secure the needle as the inlet for perfusion (supplementary Fig. I). Next, the portal vein was cannulated as the outlet with an Intramedic PE50 tube (Becton Dickinson, Franklin Lakes, NJ) connected to a silicone tube (outside diameter 1.00 mm; inside diameter 0.50 mm; 30 cm length) (supplementary Fig. I). The intestinal lymph duct was then immediately cannulated to serve as the outlet with a needle (26G) connected to a silicon tube in the same manner as for the portal vein (supplementary Fig. I), while a buffer solution (DMEM without phenol red containing 0.03% BSA) aerated with 95% O_2 and 5% CO_2 was perfused slowly from the inlet. The interval when the mice were euthanized to circulation of the infusion had to be less than 5 min.

After all three tubes were secured, perfusion was started, and the flow rate of the perfusion buffer was increased to 0.5 ml/min. The body was kept at 35°C in Krebs Ringer buffer in a water bath, and sample collection by means of gravity was started from the two outlets. We confirmed that the motility of the intestines, glucose uptake, and an appropriate ratio of lymph to portal perfusates (1:50) could be maintained for up to 90 min in our system. However, due to the fragility and sensitivity of the SI (24, 25), prolonged perfusion seems to be problematic, and the SI showed organ damage such as edema and lower motility 90 min after perfusion. Therefore, we collected samples from 10 min through 60 min after the start of perfusion. The collected samples were pooled for the analyses.

The production of HDL from the SI was examined by analyzing HDL-apo AI and apo AI using non-SDS-PAGE and SDS-PAGE, respectively, followed by Western blot analysis of apo AI in SI lymph perfusates from WT mice and ABCA1 KO mice. Peptide mapping of HDL using LC/MS and the analyses of lipid and apo composition and size distribution of HDL were performed in plasma, SI lymph perfusates, and liver perfusates from WT mice. The effects of an ABCA1 inhibitor, glyburide (26) (Cayman), and an LCAT inhibitor, DTNB (27) (Cayman), on the formation of SI-HDL were examined in WT mice by adding them to the perfusion buffer. The effects of a high-fat diet on the production of SI-HDL were examined by measuring HDL-apo AI in SI lymph perfusates using non-SDS-PAGE followed by Western blot analysis of apo AI after WT mice were fed a high-fat diet for 4 weeks.

Western blot analyses

For the analysis of apos in SI lymph perfusates, plasma, and lipoprotein density fractions, samples were run on SDS-PAGE or

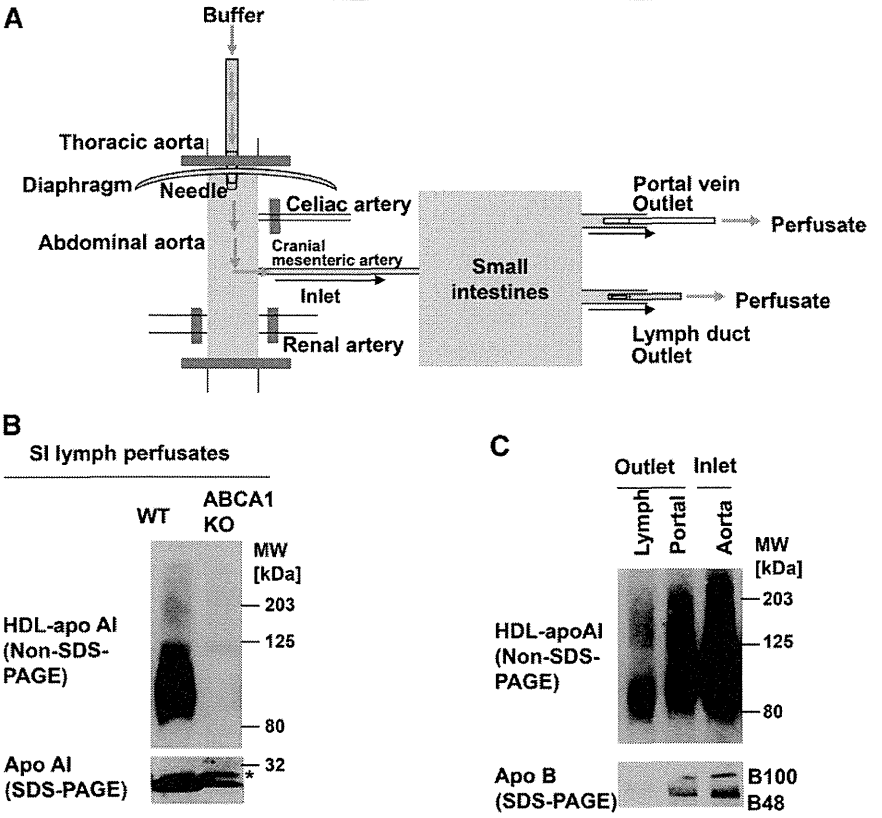

Fig. 1. Establishment of an in situ perfusion model of mouse SI and analyses of lipoproteins in the SI lymph perfusates. A: A schematic representation of our in situ perfusion system for assessing HDL production in mouse SI. The abdominal aorta and its branches were ligated as shown in red bars, and the aorta was punctured and cannulated to serve as the inlet (supplementary Fig. I). The portal vein and intestinal lymph duct were punctured and cannulated to serve as outlets. Flow of the perfusion buffer was shown by the arrows. The mouse body and perfusion buffer were warmed to 35°C before perfusion was started. B: Non-SDS-PAGE analysis of HDL-apo AI (upper panel) and SDS-PAGE analysis of apo AI (lower panel) in SI lymph perfusates from WT (left lane) and ABCA1 KO (right lane) mice. C: Non-SDS-PAGE analysis of HDL-apo AI (upper panel) and SDS-PAGE analysis of apo B48 and apo B100 (lower panel) in perfusates from the SI lymph duct and portal vein of ABCA1 KO mice perfused with buffer containing serum from WT mice.

non-SDS-PAGE, transferred to polyvinylidene difluoride membranes, and immunoblotted with anti-mouse apo AI, apo AIV, apo E, apo B100, or apo B48 overnight at 4°C. Membranes were washed and then incubated with anti-IgG antibody conjugated with HRP for 1 h at room temperature. An ECL Advance Western Blotting Detection Kit (Amersham Biosciences, Piscataway, NJ) was used for the visualization of immunoblots according to the manufacturer's protocol.

Conventional SI lymph cannulation experiments

After intraperitoneal anesthesia, the main mesenteric lymphatic duct of WT mice was cannulated as previously described by Green et al. (14). HDL was separated by ultracentrifugation from a sample of mesenteric lymph and used for the analysis of HDL proteins using LC/MS.

In situ perfusion system for the evaluation of HDL production in the liver

In situ perfusion for the liver from WT mice was performed according to the method reported by Sugano et al. (28) with minor modifications. Briefly, after the mice were deeply anesthetized, the abdomen was opened, the portal vein was cannulated in situ, and the liver was perfused with oxygenated buffer, which was the same as that used for in situ perfusion of the SI. To prevent swelling of the liver, the abdominal vena cava was incised immediately after cannulation, the thorax was opened, a part of the inferior vena cava was cut, and a cannula was inserted.

After the collected perfusate was concentrated using centrifugal filter devices (Millipore), HDL was separated by ultracentrifugation and used for the analysis of HDL proteins using LC/MS, analysis of the HDL lipid composition using HPLC, and analysis of the HDL apo composition.

MS analysis of HDL fractions

HDL fractions from mouse serum, SI lymph perfusate, SI lymph (14), and liver perfusate (28) from WT mice were buffer exchanged with 10 mM triethylammonium bicarbonate buffer (Sigma-Aldrich, St. Louis, MO) and concentrated by centrifugation (6,000 *g*, 30 min at 4°C) using Vivaspin2 (MW 3000; GE Healthcare, Buckinghamshire, UK). The protein concentration of each sample was determined with the Bradford method and adjusted to 7.5 mg/ml. Ten microliters of each sample was then subjected to reduction and alkylation [1 μl of denaturant and 2 μl of reducing reagent (AB Sciex, Foster City, CA)] for 60 min at 60°C, cystein blocking [1 μl of cystein-blocking reagent (AB Sciex)], and trypsinization [1.9 μg of trypsin (Roche, Basel, Switzerland)] for 4 h at 37°C followed by the addition of another 1.9 μg of trypsin and overnight incubation at 37°C. After digestion,

the samples were desalted and concentrated with C18 Stage tips (29) packed in-house in 60 µl of 2% acetonitrile (ACN) and 0.1% trifluoroacetic acid (TFA) buffer.

Each sample was fractionated for 70 min by HPLC (Prominence; Shimazu, Kyoto, Japan) using an SCX column [ZORBAX 5 µm 300-SCX 2.1 × 50 mm (Agilent Technologies, San Jose, CA)] at a flow rate of 10 µl/min with a KCl gradient of from 0 to 1 M in 10 mM KH_2PO_4/25% ACN solution, as described previously (30). The fractionated peptides (36 fractions) were lyophilized to dryness, and the dried peptides were reconstituted in 20 µl of 0.1% formic acid in 2% ACN and analyzed with a QSTAR Elite mass spectrometer (AB Sciex) coupled online to a nanoflow HPLC (Paradigm MS2; Michrom Bioresources, Auburn, CA) with an autosampler (HTS-PAL; CTC Analytics AG, Zwingen, Switzerland) using a nanospray ionization source (NanoSprayII; AB Sciex) that held 3 µm inner-diameter C18 columns (L-column2 ODS; Chemicals Evaluation and Research Institute, Tokyo, Japan) packed in-house into 20 cm long, 75 µm inner-diameter fused silica emitters pulled on a P-2000 Laser Based Micropipette puller (Sutter Instruments, Novato, CA). The samples were run at a flow rate of 200 nl/min with an ACN gradient (0–85 min, ACN 2%–33%; 85–95 min, ACN 33%–86%) in 0.1% formic acid.

Lipid profile analyses using HPLC

Two hundred microliters of SI lymph perfusates or HDL separated by ultracentrifugation from plasma, SI lymph perfusates, and liver perfusates from WT mice was analyzed with the HPLC system using two tandem gel permeation columns (Lipopropak XL, 7.8 mm × 300 mm; Tosoh Corp., Tokyo, Japan) at a flow rate of 700 µl/min. Total cholesterol (TC), TG, free cholesterol (FC), and phospholipid (PL) were measured with two parallel online enzymatic lipid detection systems (350 µl/min each) (Skylight Biotech, Inc., Akita, Japan) (31–34). The system was calibrated with the aid of latex beads and high-molecular-weight standards for the apparent spherical diameters of HDL.

Isolation of lipoproteins by ultracentrifugation

Lipoprotein fractions were isolated from SI lymph perfusates, SI lymph, liver perfusates, and plasma from WT mice by serial preparative ultracentrifugation as described previously (35–39). Briefly, SI lymph perfusate was overlaid with saline solution at a volume ratio of ~5:3 and ultracentrifuged at 50,000 *g* for 25 min (2.25×10^6 g/min) (40) at 10°C in a TLA-100.2 rotor in a Beckman TL-100 Tabletop Ultracentrifuge (Beckman Instruments Inc.). Chylomicron (CM) fraction (upper fraction) was collected using a tube slicer. The bottom fraction was overlaid with saline and ultracentrifuged at 100,000 rpm for 2 h at 10°C. The VLDL fraction (upper fraction) was collected using a tube slicer. The density of the d > 1.006 g/ml fraction (bottom fraction) was then adjusted to 1.063 g/ml with solid KBr and overlaid with d = 1.063 g/ml KBr solution. After centrifugation at 100,000 rpm for 2 h at 10°C, the LDL fraction (upper fraction) was collected. Finally, the density of the d >1.063 g/ml fraction (bottom fraction) was adjusted to 1.25 g/ml with solid KBr and overlaid with d = 1.25 g/ml KBr solution. After centrifugation at 100,000 rpm for 5 h at 10°C, the HDL fraction (upper fraction) was collected with a tube slicer. LDL and HDL fractions were dialyzed against saline containing EDTA (1 mM) to eliminate KBr. HDL for lipid profile analyses using HPLC and determination of protein concentration was used without dialysis.

Electron microscopy of HDL particles

The size distributions of HDL particles separated from SI lymph perfusates and plasma of WT mice were examined by electron microscopy (EM), as described previously (35). In brief, for transmission electron microscopy (TEM), HDL was separated by preparative ultracentrifugation and dialyzed against saline containing 1 mM EDTA (pH 8.0) overnight at 4°C to remove KBr. Next, HDL was dialyzed against a 10 mM NH_4HCO_3 solution for 2 h at 4°C and negatively stained with 1% uranium acetate. Electron micrographs were obtained with a computer-controlled JEOL 1200EX electron microscope (JEOL Inc., Tokyo, Japan). Images at a final magnification of 200,000× were acquired with a high-resolution digital camera. The diameters of spherical HDL particles were measured using TEM imaging Platform iTEM (Olympus Soft Imaging Solutions GmbH, Münster, Germany).

Two-dimensional gel electrophoresis

To examine the effects of LCAT inhibition on SI-HDL production, HDL in SI lymph perfusates collected using the in situ perfusion technique from WT mice with and without the presence of DTNB in the perfusion buffer was separated by native two-dimensional gel electrophoresis as described previously (41, 42). Fresh SI lymph perfusates were run on an agarose gel (0.75%) and then on a 2% to 25% polyacrylamide gel at 0°C at 100 V for 20 h. Fractionated HDL was electroblotted to a nitrocellulose sheet at 0°C and detected with the following antibodies. The first antibody was a rabbit anti-mouse apo AI antibody (BioDesign), and the second was a goat anti-rabbit IgG (DAKO) iodinated with $Na^{125}I$ by a modified chloramine T method.

Statistical data analysis

Statistical data analyses were performed using the Statistical Analysis System (SAS) Software Package (Ver. 9.2; SAS Institute Inc., Cary, NC) at Fukuoka University (Fukuoka, Japan). Differences in the lipid and protein composition of HDL between groups were examined by an ANOVA using the general linear model (43). Differences in the size of HDL particles between plasma HDL and SI-HDL were examined by the Wilcoxon rank sum test. Data are presented as the mean ± SD, and the significance level was considered to be <0.05 unless indicated otherwise.

RESULTS

Development of a novel in situ perfusion model in mice

A novel in situ perfusion model was developed in mice with isolated SI in which the arterial blood supply for the SI is blocked, leaving only the superior mesenteric artery open as the perfusion inlet for the SI. Fig. 1A shows a schematic representation of our novel in situ perfusion model. Because the source of HDL obtained from the mesenteric lymph duct of anesthetized rodents in vivo is either the secretion of HDL by SI or the filtration of HDL from plasma through the blood capillary-lymph loop into the intestinal lymph duct (19–22), in our in situ perfusion model the arterial blood supply for the SI was blocked by ligation of the abdominal aorta and its branches (Fig. 1A) to dissociate the HDL produced by the SI from HDL filtered from plasma.

The superior mesenteric artery was not ligated and was left open as the perfusion inlet (Fig. 1A). A 26G needle was inserted antegrade from the thoracic descending aorta into the abdominal aorta before ligation of the abdominal aorta and used to pump perfusion buffer through the

abdominal aorta into the mesenteric artery (Fig. 1A). The portal vein and intestinal lymph duct were punctured and cannulated to serve as outlets (Fig. 1A). Therefore, in our in situ perfusion mouse model, no further systemic blood will come into the SI after perfusion with a buffer solution starts, and thus the HDL in the infusates collected from the SI lymph duct (one of the outlets) would only be produced from the SI and not infiltrate from the systemic plasma.

The SI produces HDL

The intestine and liver are the two major sites of HDL production (15, 16, 44). To demonstrate that the SI produces HDL, SI lymph perfusates were collected from WT mice using our in situ perfusion model. Nondenaturing PAGE followed by Western blot analysis for apo AI, the major protein of HDL, clearly showed that HDL from the SI was present in SI lymph perfusate (Fig. 1B, left lane of the upper panel), but not in perfusate collected from the portal vein (data not shown). Because systemic blood does not come into the SI during perfusion due to the blockade of systemic blood by ligation of the abdominal aorta and its branches in our in situ perfusion model, this result indicates that the SI produces HDL in WT mice.

ABCA1 is required for the production of HDL from the SI

Intestinal ABCA1 has been shown to contribute to HDL biogenesis in mice in vivo (16). To clarify the influence of ABCA1 on the production of HDL from the SI, we collected lymph perfusates from ABCA1 KO mice using our in situ perfusion model. HDL-apo AI was not detected in SI lymph perfusates from ABCA1 KO mice (Fig. 1B, right lane of the upper panel). This result indicates that ABCA1 is required for the production of HDL from the SI.

However, an apo AI immunoreactive mass was detected in the form of doublets in the SI lymph perfusate from ABCA1 KO mice, in contrast to a major single band that was detected in that from WT mice (Fig. 1B, lower panel). It is possible that the upper band in ABCA1 KO mice may represent a precursor of apo AI, newly synthesized from the intestine. Therefore, the deficient HDL production from the SI of ABCA1 KO mice was not due to the defective synthesis of apo AI, but rather to the defective lipidation of apo AI (45).

Evidence that plasma HDL can filtrate from the abdominal aorta into the SI lymph duct

Although a previous study suggested that plasma HDL can infiltrate into the mesenteric lymph (16), there is still some controversy, and direct evidence is not available. We used our in situ perfusion model to clarify whether plasma lipoproteins in abdominal aorta contribute to HDL in SI lymph. Because ABCA1 KO mice showed the deficient production of HDL from the SI (Fig. 1B), the addition of serum from WT mice to the perfusion buffer should be able to show whether plasma HDL can infiltrate from the abdominal aorta to the mesenteric lymph duct.

Therefore, we used ABCA1 KO mouse bodies for in situ perfusion but added serum from WT mice to the perfusion buffer. Perfusates from the abdominal aorta (inlet) and lymph duct and portal vein (two outlets) were run on nondenaturing PAGE followed by Western blot analysis for apo AI and on SDS-PAGE followed by Western blot analysis for apo B100 and apo B48 (Fig. 1C). As shown in the upper panel of Fig. 1C, a substantial amount of HDL was present in the perfusates collected from both the SI lymph duct and the portal vein. Because SI-HDL is not formed in ABCA1 KO mice due to the defect in the lipidation of apo AI, HDL detected in SI lymph perfusates should come from the infiltration of plasma HDL from the abdominal aorta.

Apo B was detected in perfusates collected from the portal vein, but not in SI lymph perfusates (Fig. 1C, lower panel). Because no apo B was detected in SI lymph perfusates, our result indicates that apo-B-containing lipoprotein was not filtrated from the abdominal aorta into the lymph duct.

Mapping of peptides from intestinal HDL and hepatic HDL using LC/MS

A previous study has shown that HDL from the intestinal lymph duct obtained in vivo from anesthetized mice is likely to contain HDL from the systemic circulation, most of which was derived from the liver (16). Therefore, we compared the SI-HDL obtained using our novel in situ perfusion mouse model, the intestinal HDL (C-HDL) obtained in vivo from anesthetized mice using a conventional experimental procedure, and hepatic HDL (L-HDL) obtained from liver perfusion. Protein moieties of HDL from mouse plasma (P-HDL), SI-HDL, C-HDL, and L-HDL were compared by using LC/MS (**Fig. 2**).

As shown in Fig. 2, the peptide patterns of C-HDL were very similar to those of L-HDL: the same number of major peptides was detected (m/z 543, 402, 403, 523, 413, 422, and 435), and they had similar relative peptide-ion intensities. These results suggest that C-HDL may contain HDL from the systemic circulation, most of which is derived from the liver (16).

However, the peptide patterns of SI-HDL were apparently different from those of C-HDL and L-HDL: SI-HDL had additional peptides of m/z 542 and 524 that were not detected in C-HDL and L-HDL (Fig. 2B, indicated by red arrows). Because HDL obtained using our novel in situ perfusion technique is not subject to interference from the liver and plasma, our results indicate that intestinal HDL is different from hepatic HDL and that the novel in situ perfusion model is suitable for the selective evaluation for SI-HDL.

Distribution of lipids and apos in lipoproteins produced from the SI

To characterize lipoproteins produced from the SI, we examined the distribution of lipids and apos in lymph perfusates collected from WT mice using our novel in situ perfusion model. Lipid profiles were analyzed by online monitoring for TC, FC, TG, and PL after lipoproteins

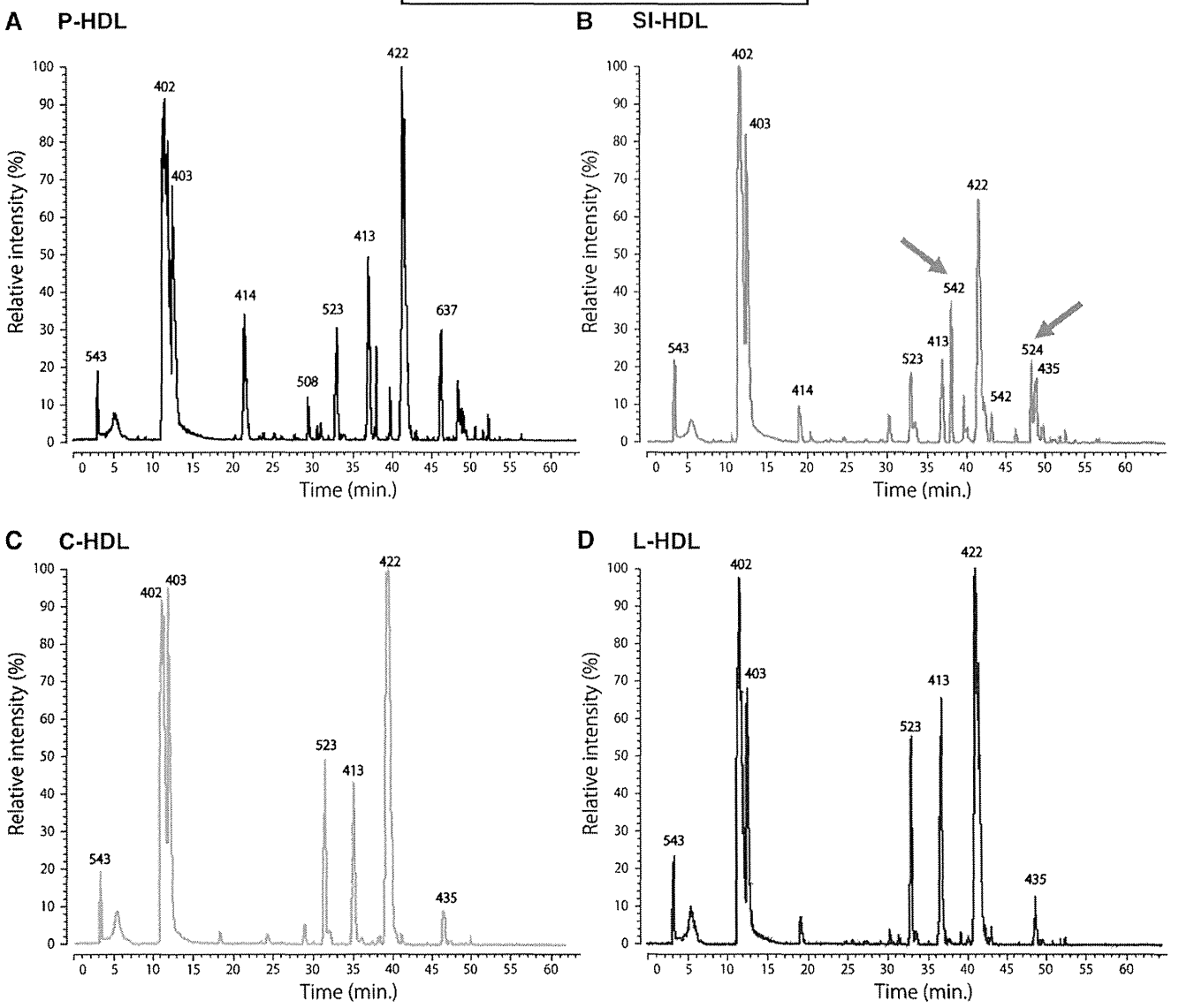

Fig. 2. Comparison of plasma HDL, intestinal HDL, and hepatic HDL in WT mice by peptide mapping using LC/MS. A–D: LC/MS total ion chromatograms of peptides, in which peptide-ion intensity is shown as a function of the peptide retention time, for HDL separated by ultracentrifugation from plasma (P-HDL) (A), SI lymph perfusates (SI-HDL) obtained using a novel in situ perfusion model (B), mesenteric lymph (C-HDL) obtained by conventional intestinal lymph cannulation experiments (C), and liver perfusates (L-HDL) (D) of WT mice. The numerical value of each peak shows *m/z* of representative peptides included in the peak. Arrows indicate peptides with *m/z* 542 and 524 detected specifically in SI-HDL.

were separated by HPLC (**Fig. 3A**). As shown in Fig. 3A, lipoproteins in SI lymph perfusates were separated into two main fractions, one corresponding to plasma HDL and another corresponding to plasma non-HDL (CM to VLDL size). The four main classes of lipids (i.e., cholesterol ester [CE], FC, TG, and PL) were mainly distributed in the non-HDL fraction (Fig. 3A), similar to plasma lipoproteins.

To examine the distribution of apos, lipoprotein density fractions (CM, VLDL, LDL, and HDL) were separated from lymph perfusates of WT mice by small-scale preparative ultracentrifugation. Apo AI, apo AIV, apo B100, and apo B48 in each lipoprotein density fraction were detected by Western blot analysis after separation by SDS-PAGE (Fig. 3B). As shown in Fig. 3B, lipoproteins produced from the SI contained only apo B48, and no apo B100, as expected (46). Apos were not detected in the LDL fraction separated from lymph perfusates (Fig. 3B), indicating that the LDL-size fraction was not produced by the SI. HDL from SI lymph perfusates contained both apo AI and AIV, similar to plasma HDL (Fig. 3B).

Lipid and protein composition of SI-HDL

WT mice were used to examine the lipid and protein composition of HDL produced from the SI. HDL was separated from plasma, SI lymph perfusates collected using our in situ perfusion model, and liver perfusates using small-scale preparative ultracentrifugation. HDL separated by ultracentrifugation was used for the measurement of total protein and apos but was further separated using HPLC for the online

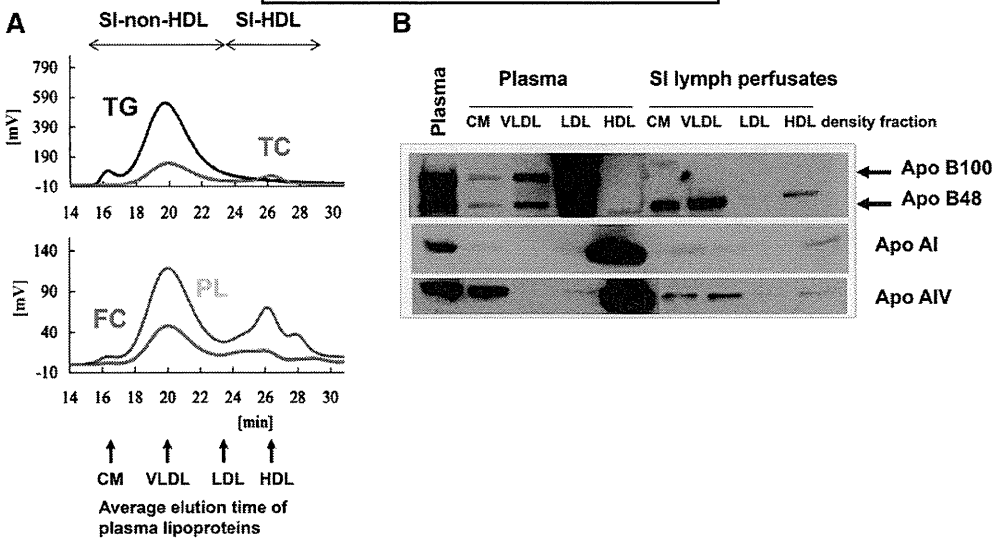

Fig. 3. HPLC analyses of lipids and preparative ultracentrifugation followed by Western blotting for apos in SI lymph perfusates. A: HPLC analyses of SI lymph perfusates from WT mice. Two hundred microliters of SI lymph perfusates was run on HPLC as described in the Methods. TC, FC, TG, and PL were measured enzymatically. Arrows denote the average elution time of indicated plasma lipoproteins in WT mice. B: Apo distribution among lipoproteins in SI lymph perfusates from WT mice separated by preparative ultracentrifugation. Lipoproteins in plasma and SI lymph perfusates were subjected to small-scale preparative ultracentrifugation to concentrate samples, and the concentrated samples were then run on SDS-PAGE followed by Western blot analysis using antibodies against the indicated apos. CM, VLDL, LDL, and HDL denote the density range of the indicated plasma lipoprotein fractions.

measurement of lipids to ensure that lipids in HDL are measured without possible interference from other lipoproteins. Supplementary Fig. II gives examples of the HPLC TC profile of HDL separated from plasma, lymph perfusates, and liver perfusates to show the purity of HDL. HPLC-separated HDL was measured for TC, TG, FC, and PL, and CE was calculated from TC and FC (47).

Table 1 and **Fig. 4A** show the contents of lipids and total protein in P-HDL, L-HDL, and SI-HDL. SI-HDL, similar to L-HDL, had a significantly higher protein content and lower lipid content than P-HDL (Table 1, Fig. 4A). CE and PL were the major lipids in SI-HDL and L-HDL, similar to P-HDL. However, the contents of CE and PL relative to protein in SI-HDL and L-HDL were significantly lower than those in P-LDL (Table 1).

Table 1 also shows the distribution of lipids in HDL. At ad libitum, SI-HDL tended to show less CE and more TG than P-HDL and L-HDL (Table 1). The distribution of CE and TG was significantly ($P < 0.05$) different between SI-HDL and L-HDL at ad libitum and between SI-HDL at ad libitum and at fasting, as assessed by a two-way ANOVA (data not shown). At fasting, TG was not detected in L-HDL but was detected in SI-HDL (Table 1).

Therefore, using our in situ perfusion model, we showed that SI-HDL was protein rich compared with HDL in plasma in WT mice and TG rich compared with L-HDL.

TABLE 1. Lipid and protein composition of HDL separated by ultracentrifugation from mouse plasma, liver perfusates, and SI lymph perfusates collected using an in situ perfusion model

	HDL in Plasma	HDL Produced from the Liver		HDL Produced from the SI	
	Ad libitum (n = 5)	Ad libitum (n = 5)	Fasting (n = 5)	Ad libitum (n = 5)	Fasting (n = 5)
HDL composition (% total mass)					
Protein	55.3 ± 2.1	83.8 ± 9.0[a]	83.3 ± 6.5[a]	86.0 ± 5.0[a]	88.8 ± 4.4[a]
Lipids	44.7 ± 2.1	16.2 ± 9.0[a]	16.7 ± 6.5[a]	14.0 ± 5.0[a]	11.2 ± 4.4[a]
FC	2.2 ± 0.5	1.0 ± 0.6[a]	1.3 ± 0.2[b]	1.3 ± 1.1	0.9 ± 0.7[a]
CE	17.9 ± 0.4	5.9 ± 2.9[a]	6.7 ± 2.9[a]	3.7 ± 2.2[a]	4.1 ± 1.8[a]
PL	24.1 ± 2.1	9.1 ± 5.5[a]	8.7 ± 3.7[a]	6.8 ± 2.2[a]	5.8 ± 3.6[a]
TG	0.5 ± 0.3	0.2 ± 0.4	0.0 ± 0.0[a]	2.3 ± 2.9	0.4 ± 0.9
HDL lipid composition (% of lipid mass)					
FC	5.0 ± 1.2	6.6 ± 6.1	8.5 ± 3.7	11.2 ± 13.4	7.0 ± 5.5
CE	40.1 ± 2.1	38.7 ± 9.8	39.3 ± 4.1	24.2 ± 14.0[a, c]	41.0 ± 18.4
PL	53.8 ± 2.3	54.2 ± 6.2	52.2 ± 2.5	50.2 ± 14.1	49.2 ± 17.9
TG	1.1 ± 0.6	0.6 ± 1.3	0.0 ± 0.0	14.3 ± 14.9[b, c]	2.8 ± 6.2

[a] $P < 0.05$, versus plasma, assessed by an ANOVA.
[b] $P < 0.1$, versus plasma, assessed by an ANOVA.
[c] $P < 0.1$, versus the liver, assessed by an ANOVA.